Large–N_C Properties of the ρ and $f_0(600)$ Mesons from Unitary Resonance Chiral Dynamics.

J. Nieves,[1] A. Pich,[1,2] and E. Ruiz Arriola[3]

[1]*Departamento de Física Teórica, IFIC, Centro Mixto Universidad de Valencia – CSIC, Edificio de Institutos de Investigación de Paterna, Aptdo. 22085, 46071, Valencia, Spain*

[2]*Physik-Department and TUM Institute for Advanced Study, Technische Universität München, D-85748 Garching, Germany*

[3]*Departamento de Física Atómica, Molecular y Nuclear and Instituto Carlos I de Física Teórica y Computacional, Universidad de Granada, E-18071 Granada, Spain.*

(Dated: July 19, 2011)

We construct $\pi\pi$ amplitudes that fulfill exact elastic unitarity, account for one loop Chiral Perturbation Theory contributions and include all $1/N_C$ leading terms, with the only limitation of considering just the lowest-lying nonet of exchanged resonances. Within such scheme, the N_C dependence of σ and ρ masses and widths is discussed. Robust conclusions are drawn in the case of the ρ resonance, confirming that it is a stable meson in the limit of a large number of QCD colors, N_C.

Less definitive conclusions are reached in the scalar-isoscalar sector. With the present quality of data, we cannot firmly conclude whether or not the $N_C = 3$ $f_0(600)$ resonance completely disappears at large N_C or it has a sub-dominant component in its structure, which would become dominant for a number of quark colors sufficiently large.

PACS numbers: 11.15.Pg, 12.39.Fe, 13.75.Lb,12.39.Mk

Keywords: Meson Resonances, Unitarity, Large N_C, Chiral Symmetry, Low Energy Constants and Resonance Saturation

arXiv:1107.3247v1 [hep-ph] 16 Jul 2011

I. INTRODUCTION

Light $J^P = 0^+$ scalar resonance properties are of great interest, since they might help to unravel details of QCD chiral symmetry breaking and confinement. Despite many theoretical efforts, the current understanding of the microscopic structure of these resonances is still far from being complete. The difficulty is triggered by the fact that scalar mesons carry vacuum quantum numbers, and also because strong final-state interactions hide their underlying nature when they are produced. Among other resonances, the lightest one $f_0(600)$, currently denoted as the σ meson, is an essential ingredient of the nuclear force, as anticipated long ago [1]. Its contribution to the mid-range nuclear attraction provides saturation and binding in atomic nuclei. During many years, there has been some arbitrariness on the "effective" scalar meson mass and coupling constant to the nucleon, partly stimulated by lack of other sources of information. The existence of this broad low-lying state is by now out of question; its mass and width have accurately been extracted from data analysis incorporating a large body of theoretical and experimental constraints [2–4]. The debate on the nature of the σ meson is nonetheless not completely over. Structures of the tetraquark or glueball type have been proposed (see e.g. Ref. [5] for a recent review and references therein). It is remarkable that such an accurately determined state is so poorly understood from the more fundamental point of view of the underlying QCD dynamics of $N_C \times N_F$ quarks and $N_C^2 - 1$ gluons, where $N_C = 3$ is the number of color species and N_F is the number of flavors. To clarify the issue on the nature of the σ meson, it has been suggested to follow the dependence on a variable number of colors $N_C \neq 3$ of its mass and width [6] by assuming that hadronic properties scale similarly as if N_C was large. A prerequisite for this scaling approach to work is that at least *all leading–N_C* effects are taken into account.

The limit of an infinite number of quark colors keeping $\alpha_s N_C$ fixed (α_s is the strong coupling constant), turns out to be a very useful and simplifying starting point to understand many qualitative features of the strong interaction [7, 8]. While keeping essential properties of Quantum Chromodynamics (QCD), under the assumption of confinement, the large–N_C limit provides a weak coupling regime to perform quantitative QCD studies. In this work we are interested in describing the large–N_C scaling of $\pi\pi$ scattering and the induced large–N_C behavior of two-pion resonances. At leading order in $1/N_C$, the meson-meson scattering amplitudes are given by sums of tree diagrams induced by the exchange of an infinite number of weakly interacting physical (stable) hadrons. Indeed, meson and glueball masses scale as $\mathcal{O}(N_C^0)$ whereas the widths do as $\mathcal{O}(1/N_C)$ and $\mathcal{O}(1/N_C^2)$, respectively. Crossing symmetry implies that this sum is the tree-level approximation to some local effective relativistically-invariant Lagrangian, which by assuming that confinement still holds at large N_C, can be re-written in terms of mesonic fields and hence complies with quark-hadron duality. Higher-order $1/N_C$ corrections correspond to hadronic loop diagrams and effectively restore unitarity in the time-like region.

Resonance Chiral Theory (RχT) [9, 10] includes the pseudo-Goldstone bosons and the resonances as dynamically active degrees of freedom of the theory. The low-energy limit of RχT must comply with low-energy theorems based on Chiral Perturbation Theory (ChPT) [11–13], and this property has been used to predict systematically the Low Energy Constants (LECs) of ChPT in terms of masses and couplings of the resonances, when integrating them out of the action, at the chiral orders $\mathcal{O}(p^4)$ [9] and $\mathcal{O}(p^6)$ [14]. The ChPT Lagrangian includes the octet of pseudo-Goldstone bosons, however, when extending ChPT, RχT incorporates the resonances as active degrees of freedom that are included in nonets, since octet and singlet of a $SU(N_F = 3)$ group

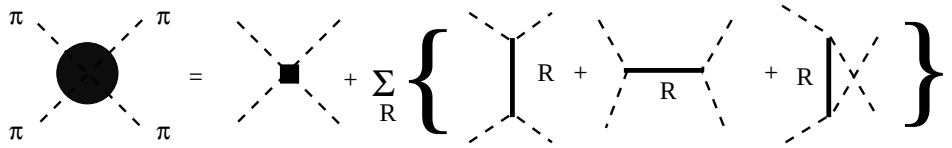


FIG. 1: Leading large–N_C $\pi\pi$ scattering diagrams made of contact (polynomial) and resonance-exchange (pole) terms in t, s and u channels.

merge into a nonet for $N_C \to \infty$. The ChPT Lagrangian is built using the spontaneously-broken chiral symmetry of massless QCD. The explicit symmetry breaking from non-zero quark masses and electromagnetic interactions is incorporated in exactly the same way as it happens in QCD. The nonets of resonances are added requiring the general properties and invariance under charge conjugation and parity, and the structure of the operators is determined by chiral symmetry. At first order in the $1/N_C$ expansion, terms with more than one trace and loops are suppressed. The first property permits to postpone some terms allowed by the symmetries as subleading. However, the theory determined by just symmetries does not share yet some of the known properties of QCD at high energies or accepted from hadronic Regge phenomenology[1]. Further constraints on the couplings arise by matching the interpolating resonance theory at intermediate energies with asymptotic QCD at the level of Green functions and/or form factors. The application of these properties determines a series of relations between the couplings of RχT, reducing the number of couplings and enhancing the predictability. We remind here that QCD, besides current quark masses, has only one dimensionful parameter, $\Lambda_{\rm QCD}$. Of course, there are infinitely many such short-distance constraints and hence a sufficiently large number of states may eventually be needed to avoid contradictory results [15].

A further and less trivial question is related to whether or not purely contact terms should be regarded as independent of exchange terms in the large–N_C framework. Within $\pi\pi$ scattering, this corresponds to distinguish between contact 4π vertices and those where a resonance field propagates between 2π states (see Fig. 1). While the large–N_C expansion is expected to provide a better approximation to data in the space-like region where unitarity does not play an active role, the approach is not specifically related to a given energy range. This means that if the tower of *all* infinitely many states is included, the question on the duality between contact and exchange terms is pertinent. However, if the exchanged resonance spectrum is truncated above a given energy, contact terms must necessarily arise to encode the explicitly disregarded high-energy contributions while still complying to the short-distance constraints [10]. The explicit values of the contact LECs depend on the functional parametrization adopted for the resonance fields.

In the Single-Resonance-Approximation (SRA) scheme, each infinite resonance sum is just approximated by the contribution from the lowest-lying meson multiplet with the given quantum numbers. This is meaningful at low energies where the contributions from higher-mass states are suppressed by their corresponding propagators. The SRA corresponds to work with a low-energy Effective Field Theory (EFT) below the scale of the second resonance multiplets. In this work, we will use the SRA of RχT to re-analyze how the σ and ρ properties depend on N_C, mainly based on the study of $\pi\pi$ scattering. An early investigation was proposed in Refs. [16, 17] keeping the leading $1/N_C$ contributions but omitting the ChPT chiral logarithms. We impose leading–N_C short-distance constraints, as discussed in detail in Refs. [10, 18]. This turns out to be of capital importance because it leads to a clear distinction between leading and subleading N_C contributions to the $\pi\pi$ amplitudes. It also allows for a meaningful extension of the framework to the $N_C > 3$ world. Besides, enforcing the short-distance constraints reduces the number of free parameters to only the subtraction constants, needed to restore exact elastic unitarity, and the masses of the exchanged resonances. In addition, we check that a direct analysis of $\pi\pi$ scattering at leading order in $1/N_C$ and using high-energy constraints, based on forward dispersion relations and Regge phenomenology, generates relations between the resonance properties compatible with those already obtained in [10, 18] by looking at other processes.

We will first construct $\pi\pi$ amplitudes that fulfill exact elastic unitarity, account for one-loop ChPT contributions, and include all $1/N_C$ leading terms in the SRA. Next, we will look for poles in the appropriate unphysical sheets of the amplitudes, and discuss their properties when N_C deviates from its physical value,[2] to learn details on their nature. In this manner, we improve on previous analyses [6, 20–22] where leading $1/N_C$ terms, beyond a certain order in the chiral expansion, were neglected.

On the other hand, in the strict chiral and large–N_C limits, the pseudo-scalar singlet η_1 and the π are degenerate [23–25]. The interplay between ChPT and large N_C has been addressed in Ref. [26]. $U(3)$ meson-meson scattering has been treated in [27] with only contact $\mathcal{O}(p^2)$ chiral interactions. In Ref. [28], in addition to the contact $\mathcal{O}(p^2)$, the leading–N_C scalar resonance exchange has been included, but leaving aside the vector meson exchange. This latter mechanism not only contributes to the

[1] Regge behavior, while not directly deduced from QCD, works rather well and it has played a decisive role in the benchmark and unprecedented accurate determination of the σ meson mass and width [2–4], by extending the high energy region above $\sqrt{s} > 1.4$ GeV.

[2] We will focus here on the properties of the poles in the complex s plane. The N_C behavior of the Breit-Wigner resonance parameters has been discussed, in a model independent manner, at length in Ref. [19], and we refer the reader to this latter work for further details.

P-waves, but also to other S-wave channels via the left-cut contribution. Recently, a full-fledged one-loop unitarized couple-channel $U(3)$ calculation, including both scalar and vector resonance exchanges, has been undertaken in Ref. [29]. Besides achieving an excellent description of phase shifts until center-of-mass energies of around 1.4 GeV, this reference also analyzes the N_C behavior of the amplitudes. Among other results, it is explicitly shown there that when N_C increases, the mass of the lowest eigenstate of the η_1–η_8 mass matrix decreases, reaching values of around twice the pion mass in the $N_C = 30$ region. Thus, a natural question arises here, namely, do the η–η' degrees of freedom play a relevant role to determine the N_C trajectory of the σ and ρ resonances? This is addressed also in Ref. [29], from where one might infer that this is certainly not the case. Those degrees of freedom turn out to be much more relevant in the study of the N_C dependence of masses and widths of higher resonances, as for instance the $f_0(980)$. We benefit here from this observation, and we will neglect η–η' effects in what follows.

We should also point out that some aspects of the $N_C \neq 3$ extension undertaken in Ref. [29] deserve discussion, and we believe they can be improved along the lines followed in this paper. In particular, the leading $1/N_C$ contributions were not properly considered in Ref. [29]. As a consequence, we cannot firmly conclude a scenario where the σ moves far away in the complex plane for large N_C, as obtained in [29]. We will give some more details below Eq. (56). Note that crossing symmetry, the possible absence of an exotic isotensor ($I = 2$) state and the well-established fact that the ρ width decreases with N_C imply the existence of a narrow scalar-isoscalar resonance, in the large–N_C limit, with a mass comparable to that of the ρmeson [30].

The paper is organized as follows. In Section II we introduce our notation in order to make the paper self-contained. We also review some important features of $\pi\pi$ forward dispersion relations and crossing symmetry, which yield to two sum rules, keeping an eye on the large–N_C expansion. In Section III we discuss the $\pi\pi$ scattering amplitude in the SRA of RχT and analyze high-energy conditions which yield to the short-distance constraints. In Section IV, the $\mathcal{O}(p^4)$ ChPT contributions to the $\pi\pi$ scattering amplitude and its matching to the leading $1/N_C$ piece are discussed. Actually, we manage to write an amplitude which is correct to $\mathcal{O}(p^4)$ and includes, within the SRA, the leading $\mathcal{O}(1/N_C)$ terms to all orders in the chiral expansion. However, it still needs to be unitarized before being confronted to scattering data. After unitarization, we fix our parameters in Section V by fitting the $(I,J) = (0,0)$, $(1,1)$ and $(2,0)$ phase shifts in the real $N_C = 3$ world. This complies with the determination of the RχT Lagrangian parameters at the leading–N_C approximation. Only then do we allow ourselves to analyze the $N_C > 3$ situation in Section VI and the emerging picture for $\pi\pi$ resonances as the number of colors is varied. Finally, in Section VII we draw the main conclusions of our work.

II. GENERAL FEATURES OF $\pi\pi$ SCATTERING

A comprehensive presentation of $\pi\pi$ scattering can be seen at the textbook level [31] and more recently in [32]. We summarize here the relevant formulae to fix our notation and to provide a proper perspective of our subsequent analysis merging large N_C, ChPT and unitarity considerations.

A. Kinematics

The $\pi_a(p_1) + \pi_b(p_2) \to \pi_c(p_1') + \pi_d(p_2')$ scattering amplitude is written as

$$T_{ab;cd} = A(s,t,u)\delta_{ab}\delta_{cd} + A(t,s,u)\delta_{ac}\delta_{bd} + A(u,t,s)\delta_{ad}\delta_{bc}\,, \tag{1}$$

with the standard choice of Mandelstam variables $s = (p_1+p_2)^2$, $t = (p_1-p_1')^2$ and $u = (p_1-p_2')^2$, where $A(s,t,u)$ is the $\pi^+\pi^- \to \pi^0\pi^0$ amplitude, which is the only independent amplitude thanks to isospin, crossing and Bose-Einstein symmetries. That is, if $T_{I_s}(s,t,u)$ is the isospin combination with total isospin I (in the s-channel), one has,

$$T_{I_s=0}(s,t,u) = \frac{1}{2}\left\{3A(s,t,u) + A(t,s,u) + A(u,t,s)\right\}, \tag{2}$$

$$T_{I_s=1}(s,t,u) = \frac{1}{2}\left\{A(t,s,u) - A(u,t,s)\right\}, \tag{3}$$

$$T_{I_s=2}(s,t,u) = \frac{1}{2}\left\{A(t,s,u) + A(u,t,s)\right\}. \tag{4}$$

For the normalization we will use here the conventions from [33]. The partial-wave decomposition in the s-channel becomes

$$T_I(s,t,u) = \sum_{J=0}^{\infty}(2J+1)T_{IJ}(s)P_J(\cos\theta)\,, \tag{5}$$

where $T_{IJ}(s)$ is the projection of the $\pi\pi$ elastic scattering amplitude with given total isospin I and angular momentum J:

$$\begin{aligned} T_{IJ}(s) &= \frac{1}{2}\int_{-1}^{+1} d\cos\theta\, P_J(\cos\theta)\, T_I\left(s,t(s,\cos\theta),u(s,\cos\theta)\right) \\ &= -16\pi\left(\frac{\eta_{IJ}(s)e^{2i\delta_{IJ}(s)}-1}{2i\rho(s)}\right), \end{aligned} \tag{6}$$

with

$$\rho(s)=\sqrt{1-\frac{4m_\pi^2}{s}}, \tag{7}$$

being $m_\pi = 139.57$ MeV the pion mass and P_J the Legendre polynomials. The in-elasticity $\eta_{IJ}(s)=1$ for $s<16m_\pi^2$ and $\eta_{IJ}(s)<1$ for $s>16m_\pi^2$. Besides, δ_{IJ} are the phase shifts and the Mandelstam variables t and u depend on s and on θ, the scattering angle in the center-of-mass frame (c.m.). The optical theorem reads

$$\sigma_I(s) = -\frac{1}{s\rho(s)}\,\mathrm{Im}T_I(s,0,4m_\pi^2-s) = \sum_J \sigma_{IJ}(s), \tag{8}$$

where the partial-wave total cross section is defined as

$$\sigma_{IJ}(s)=16\pi\frac{(2J+1)}{s-4m_\pi^2}\left[\eta_{IJ}\sin^2\delta_{IJ}+\frac{1}{2}(1-\eta_{IJ})\right]. \tag{9}$$

This value is bound by

$$\sigma_{IJ}(s)\le 8\pi(2J+1)\frac{1+\eta_{IJ}}{s-4m_\pi^2}. \tag{10}$$

The contribution of a resonance state, with spin J and isospin I, to the partial cross section in the narrow-width limit and assuming $m_{IJ}^2 \gg 4m_\pi^2$ reads,

$$\sigma_{IJ}(s)=(2J+1)\,\frac{16\pi^2\Gamma_{IJ}}{m_{IJ}}\,\delta(s-m_{IJ}^2). \tag{11}$$

Of course, one may think that such a limit does not apply to a broad state as the σ. Within a Breit-Wigner model, the finite width correction effectively corresponds to a reduction $\Gamma\to\Gamma[1-\Gamma/(\pi m)]$, which even for the extreme case $\Gamma=m$ yields to a moderate 30% correction.

Using the recent GKPRY parameterizations of Ref. [34] for the partial S, P, D and F waves, cross sections are presented in Fig. 2 up to $\sqrt{s}\le 1.42$ GeV. As we see, the S0, P and D0 waves play an outstanding role featuring the appearance of the $f_0(600)$, $\rho_1(770)$, $f_0(980)$ and $f_2(1270)$ resonances. Below the $\bar{K}K$ production threshold, $s_{\bar{K}K}=4m_K^2$, only S0 and P are essential.

B. Crossing and forward dispersion relations

In the (crossed) t-channel the amplitudes read

$$\begin{pmatrix} T_{I_t=0}(s,t,u)\\ T_{I_t=1}(s,t,u)\\ T_{I_t=2}(s,t,u)\end{pmatrix} = \begin{pmatrix} \frac{1}{3} & 1 & \frac{5}{3}\\ \frac{1}{3} & \frac{1}{2} & -\frac{5}{6}\\ \frac{1}{3} & -\frac{1}{2} & \frac{1}{6}\end{pmatrix}\begin{pmatrix} T_{I_s=0}(s,t,u)\\ T_{I_s=1}(s,t,u)\\ T_{I_s=2}(s,t,u)\end{pmatrix}, \tag{12}$$

where I_t and I_s are the corresponding isospins in the t- and s-channels respectively.

The rigorous Froissart bound from axiomatic field theory requires that in the forward direction ($t=0$) these amplitudes, up to logarithmic corrections, are asymptotically polynomially bound by a single power of s. Actually, in terms of the crossing-odd variable $\nu=(s-u)/2$, the amplitude $T_{I_t}(\nu,t)\equiv T_{I_t}(\nu+2m_\pi^2-t/2,t,-\nu+2m_\pi^2-t/2)$ satisfies $T_{I_t}(-\nu,t)=(-)^{I_t}T_{I_t}(\nu,t)\to\nu^{n_{I_t}}$, with $n_{I_t}\le 1$ when $\nu\to\infty$. This means that a forward ($t=0$) once-subtracted dispersion relation is fulfilled, by considering a closed contour excluding the cuts $-\infty<\nu<-2m_\pi^2$ and $2m_\pi^2<\nu<+\infty$ (see Fig. 3), where $T(\nu+i0^+)-T(\nu-i0^+)=$

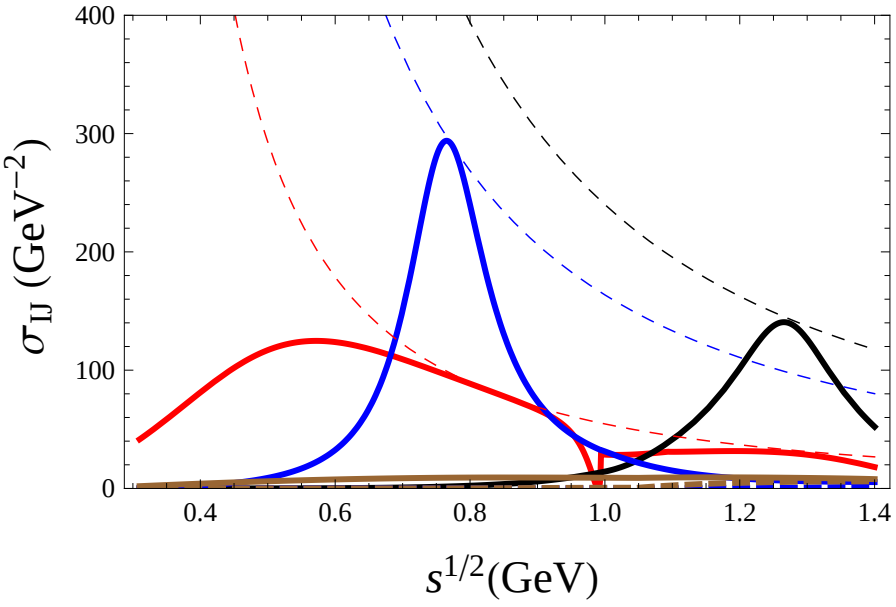


FIG. 2: (Color online) The total partial-wave cross sections $\sigma_{IJ}(s)$ (in GeV^{-2}), defined as a function of the cm energy variable $\sqrt{s}$ (in GeV) for the S0 (Solid, Red), D0 (Solid, Black), P (Solid, Blue), F (Dashed, Blue), S2 (Solid, Brown) and D2 (Dashed, Brown) partial waves below $\sqrt{s} = 1.42$ GeV, from the GKPRY parameterization with set UFD of parameters given in [34]. We also draw the unitarity bounds (dashed lines) for S0 (red), P (blue) and D2 (black) waves, using $\eta_{00} = \eta_{11} = 1$ and $\eta_{02} = 0.88$ respectively.

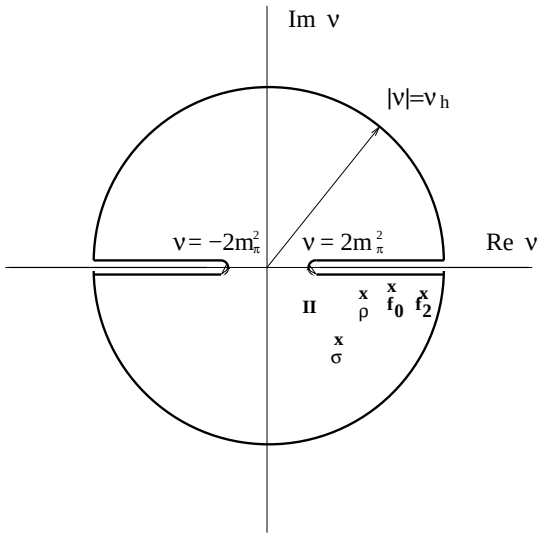


FIG. 3: The contour in the complex crossing-odd ν plane used to derive FDRs for the t-channel isospin $\pi\pi$ scattering amplitude. For $t = 0$ $\nu = s - 2m_\pi^2$, so that $\nu = 2m_\pi^2$ corresponds to the $\pi\pi$ threshold. The principal value of the forward scattering amplitude corresponds to $T_t(\nu + i0^+)$. Finite Energy Sum Rules arise for the Regge-subtracted amplitude for the finite circle $|\nu| \leq \nu_h$. Low-lying resonances $f_0(600) \equiv \sigma$, $\rho_1(770)$, $f_0(980)$ and $f_2(1275)$ are also marked by crosses in the Second Riemann Sheet, across the cut.

$2i\,\mathrm{Im}T(\nu + i0^+) \equiv 2i\,\mathrm{Im}T(\nu)$. The subtraction constant can be fixed at low energies, and more specifically at $\nu = 0$ or equiva-

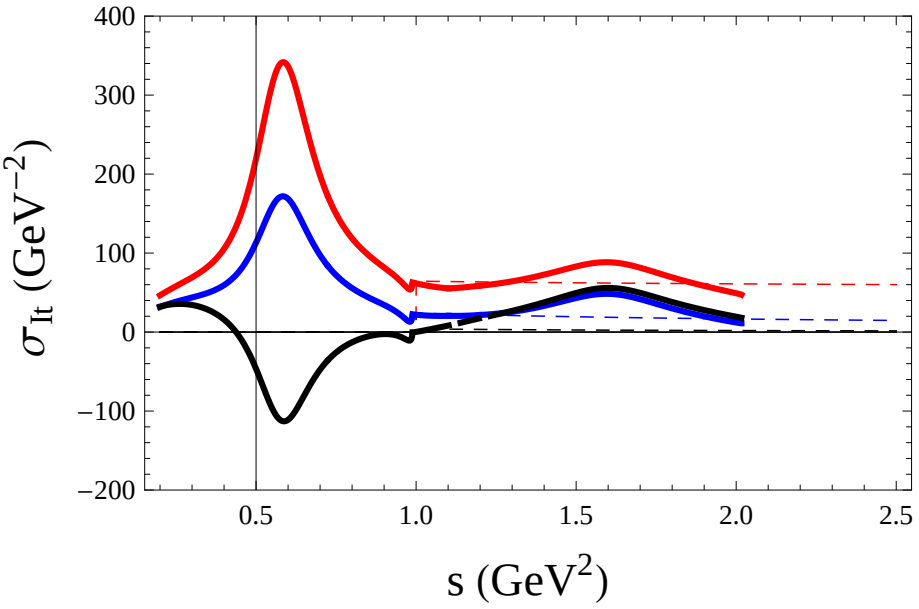


FIG. 4: The $I_t = 0,1,2$ total cross sections, as a function of the s variable, including S, P, D and F waves below $\sqrt{s} = 1.42$ GeV (solid lines) and the corresponding Regge behavior starting at $\sqrt{s} = 1.42$ GeV (dashed lines) used in the solutions of Ref. [34]. $I_t = 0$ (Red), $I_t = 1$ (Blue) and $I_t = 2$ (Black).

lently $s = 2m_\pi^2$, i.e. below threshold. Thus, at $t = 0$, we get the Forward Dispersion Relations (FDRs):

$$\begin{aligned}
T_{I_t=0}(\nu,0) &= T_{I_t=0}(0,0) + \frac{2\nu^2}{\pi}\int_{2m_\pi^2}^{\infty}\frac{d\nu'}{\nu'}\frac{\mathrm{Im}T_{I_t=0}(\nu',0)}{\nu'^2-\nu^2}\,,\\
\frac{T_{I_t=1}(\nu,0)}{\nu} &= \lim_{\nu_0\to 0}\frac{T_{I_t=1}(\nu_0,0)}{\nu_0} + \frac{2\nu^2}{\pi}\int_{2m_\pi^2}^{\infty}\frac{d\nu'}{\nu'^2}\frac{\mathrm{Im}T_{I_t=1}(\nu',0)}{\nu'^2-\nu^2}\,,\\
T_{I_t=2}(\nu,0) &= T_{I_t=2}(0,0) + \frac{2\nu^2}{\pi}\int_{2m_\pi^2}^{\infty}\frac{d\nu'}{\nu'}\frac{\mathrm{Im}T_{I_t=2}(\nu',0)}{\nu'^2-\nu^2}\,.
\end{aligned} \tag{13}$$

The absorptive part of the amplitude can be written as an optical theorem in the ν variable:

$$\mathrm{Im}T_{I_t}(\nu,0) = -\sqrt{\nu^2-4m_\pi^4}\;\sigma_{I_t}(\nu)\,, \tag{14}$$

where one goes from I_t to I_s with the same s–t crossing matrix as for the amplitudes, see Eq. (12). The FDRs converge, provided $|\mathrm{Im}T_{I_t}(\nu,0)| < \nu^a$ with $a < 2$, for large values of ν. Results for σ_{I_t} are presented in Fig. 4, up to $\sqrt{s} = 1.42$ GeV, using the UFD parameterization of Ref. [34] for the partial S, P, D and F waves

These general constraints are obeyed for any Quantum Field Theory and by QCD in particular. On the other hand, for $t \neq 0$, and sufficiently large ν, say $\nu > \nu_h$, one has the phenomenologically successful Regge behavior given by[3]

$$\mathrm{Im}T_{I_t}(\nu,t) \to -2\pi^2\sum\beta_{I_t}(t)\left[\frac{\nu}{\nu_0}\right]^{\alpha_{I_t}(t)}\,, \tag{15}$$

where $\sum$ indicates summation over several Regge trajectories, which for small t are given by $\alpha_{I_t}(t) = \alpha_{I_t}(0) + t\alpha'_{I_t} + \ldots$ The slope parameter, $\alpha'_{I_t}(0) \sim 1/(2m_\rho^2) = 0.9$ GeV^{-2} is nearly universal and the leading trajectory intercepts are $\alpha_0(0) \sim 1$, $\alpha_1(0) \sim 1/2$ and $\alpha_2(0) \sim 0$ (for a review within a modern $\pi\pi$ context see e.g. Refs. [35, 36] and references therein). We also show in Fig. 4

[3] Our amplitude and that used ($F(\nu,t)$) in Ref. [34] are related by $T(\nu,t) = -2\pi^2 F(\nu,t)$.

the Regge behavior used in the construction of the partial waves via FDRs, Roy and GKPY equations.[4] As we see, there is some mismatch between the partial waves and the Regge behavior. This is somewhat expected, since Regge behavior provides an average of the oscillating resonance contribution in the high-energy region. The region $\sqrt{s} < 1.42$ GeV is well described by S, P, D and F waves, since the exchanged ρ meson in the t-channel corresponds to longest range $1/m_\rho$ and hence $J_{\max} \sim \sqrt{s}/m_\rho$.

C. Finite Energy Sum Rules

Separating the Regge tail in the dispersive integral, corresponding to the integration region $\nu' > \nu_h$, we have for $I_t = 0, 2$, in the limit $\nu \to +\infty$ and assuming $\alpha_{I_t}(0) < 2$,

$$\begin{aligned} T_{I_t}(\nu,0)|_{\text{Regge}} &\equiv \frac{2\nu^2}{\pi}\int_{\nu_h}^{\infty}\frac{d\nu'}{\nu'}\frac{\left[-2\pi^2\sum\beta_{I_t}(0)\,(\nu'/\nu_0)^{\alpha_{I_t}(0)}\right]}{\nu'^2-\nu^2-\mathrm{i}\varepsilon} \\ &= 2\pi^2\sum\frac{\beta_{I_t}(0)}{\sin\left(\frac{\alpha_{I_t}(0)\pi}{2}\right)}e^{-\mathrm{i}\alpha_{I_t}(0)\pi/2}\left(\frac{\nu}{\nu_0}\right)^{\alpha_{I_t}(0)} - 4\pi\sum\frac{\beta_{I_t}(0)}{\alpha_{I_t}(0)}\left(\frac{\nu_h}{\nu_0}\right)^{\alpha_{I_t}(0)} + \mathscr{O}(\nu_0/\nu) \end{aligned} \tag{17}$$

and similarly for $I_t = 1$,

$$\begin{aligned} \left.\frac{T_{I_t=1}(\nu,0)}{\nu}\right|_{\text{Regge}} &\equiv \frac{2\nu^2}{\pi}\int_{\nu_h}^{\infty}\frac{d\nu'}{\nu'^2}\frac{\left[-2\pi^2\sum\beta_{I_t=1}(0)\,(\nu'/\nu_0)^{\alpha_{I_t=1}(0)}\right]}{\nu'^2-\nu^2-\mathrm{i}\varepsilon} \\ &= \left(2\pi^2\sum\frac{\beta_{I_t=1}(0)}{\sin\left(\frac{\hat\alpha\pi}{2}\right)}e^{-\mathrm{i}\hat\alpha\pi/2}\left(\frac{\nu}{\nu_0}\right)^{\hat\alpha} - 4\pi\sum\frac{\beta_{I_t=1}(0)}{\hat\alpha}\left(\frac{\nu_h}{\nu_0}\right)^{\hat\alpha}\right)\frac{1}{\nu_0} + \mathscr{O}(1/\nu)\,, \end{aligned} \tag{18}$$

with $\hat\alpha = \alpha_{I_t=1}(0) - 1$. Note that the last term in both Eqs. (17) and (18) is a constant subleading contribution. We will denote this constant term as $-R_{I_t}$. Requiring

$$T_{I_t}(\nu,0) \;\to\; 2\pi^2\sum\frac{\beta_{I_t}(0)}{\sin\left(\frac{\alpha_{I_t}(0)\pi}{2}\right)}e^{-\mathrm{i}\alpha_{I_t}(0)\pi/2}\left(\frac{\nu}{\nu_0}\right)^{\alpha_{I_t}(0)}, \quad I_t = 0,2\,, \tag{19}$$

$$\frac{T_{I_t=1}(\nu,0)}{\nu} \;\to\; \frac{2\pi^2}{\nu_0}\sum\frac{\beta_{I_t=1}(0)}{\sin\left(\frac{\hat\alpha\pi}{2}\right)}e^{-\mathrm{i}\hat\alpha\pi/2}\left(\frac{\nu}{\nu_0}\right)^{\hat\alpha}, \tag{20}$$

in the $\nu \to +\infty$ limit, we get the Finite Energy Sum Rules (FESRs)

$$\begin{aligned} T_{I_t=0}(0) &= -\frac{2}{\pi}\int_{2m_\pi^2}^{\nu_h} d\nu\sqrt{1-\frac{4m_\pi^4}{\nu^2}}\,\sigma_{I_t=0}(\nu) + R_{I_t=0}\,, \\ T'_{I_t=1}(0) &= -\frac{2}{\pi}\int_{2m_\pi^2}^{\nu_h}\frac{d\nu}{\nu}\sqrt{1-\frac{4m_\pi^4}{\nu^2}}\,\sigma_{I_t=1}(\nu) + R'_{I_t=1}\,, \\ T_{I_t=2}(0) &= -\frac{2}{\pi}\int_{2m_\pi^2}^{\nu_h} d\nu\sqrt{1-\frac{4m_\pi^4}{\nu^2}}\,\sigma_{I_t=2}(\nu) + R_{I_t=2}\,, \end{aligned} \tag{21}$$

[4] For our purposes we need the following Regge tails [34], valid for $s > s_h = (1.42\text{ GeV})^2$:

$$\begin{aligned} \mathrm{Im}T_{I_t=0}(\nu,0) &= -2\pi^2\left[b_P(\nu/\nu_0) + b_{P'}(\nu/\nu_0)^{a_{P'}}\right], \\ \mathrm{Im}T_{I_t=1}(\nu,0) &= -2\pi^2 b_1(\nu/\nu_0)^{a_1}\,, \\ \mathrm{Im}T_{I_t=2}(\nu,0) &= -2\pi^2 b_2(\nu/\nu_0)^{a_2}\,. \end{aligned} \tag{16}$$

The numerical values of the parameters are given in section 8 of the appendix A of Ref. [34].

where

$$
\begin{aligned}
R_{I_t=0} &= 4\pi b_P \left(\frac{\nu_h}{\nu_0}\right) + 4\pi \frac{b_{P'}}{a_{P'}} \left(\frac{\nu_h}{\nu_0}\right)^{a_{P'}}, \\
R'_{I_t=1} &= \frac{4\pi b_1}{a_1 - 1} \frac{1}{\nu_h} \left(\frac{\nu_h}{\nu_0}\right)^{a_1}, \\
R_{I_t=2} &= 4\pi \frac{b_2}{a_2} \left(\frac{\nu_h}{\nu_0}\right)^{a_2}.
\end{aligned} \tag{22}
$$

For $\sqrt{s_h} = \sqrt{\nu_h + 2m_\pi^2} = 1.42$ GeV, we get the values $T_{I_t=0}(0) = -121.8 + 64.3\,(P) + 28.2\,(P') = -29.3$, $T'_{I_t=1}(0) = -105.2 - 19.4\,(\rho)$ GeV$^{-2} = -124.6$ GeV^{-2} and $T_{I_t=2}(0) = -12.25 + R_{I_t=2}$. Indeed, in the window $\sqrt{\nu_h} \in (1, 1.42)$ GeV, we observe a smooth ν_h dependence of both the integral and the R_{I_t} contributions.[5] Moreover, the total sum itself remains fairly independent of ν_h, as well. Being more quantitative the right-hand side of Eqs. (21) changes at the level of 10% and 4% for the $I_t = 0$ and 1 cases, respectively, when $\sqrt{\nu_h}$ varies in the interval (1,1.42) GeV. For the case $I_t = 1$, $R'_{I_t=1}$ amounts, at energies as small as 1 GeV, to around 25% of the total, and decreases with increasing ν_h, as deduced from its Regge behavior. For the case of $I_t = 2$, the integral contribution shows a more pronounced dependence on ν_h, and it changes sign at around half of the (1,1.42) GeV interval. However, this contribution in size is just at maximum around one third of that of $R_{I_t=2}$, which is almost constant, because of the smallness of the Regge intercept, a_2. Furthermore, the sign of $R_{I_t=2}$ depends on the sign of a_2 and actually the FESR becomes ambiguous for $a_2 = 0$, since the amplitude would show a logarithmic growth $\sim \log(-\nu^2/\nu_h^2)$ instead of a Regge behavior. For a diverging/converging amplitude we have a positive/negative contribution to the sum rule. These ambiguous signs appear in the CFD and UFD solutions of Ref. [34], from where one gets $R_{I_t=2} = -30(30)$ and $R_{I_t=2} = 20(40)$, respectively, both results compatible with zero.

D. Adler and σ Sum rules

If $R'_{I_t=1}$ and $R_{I_t=2}$ are neglected in Eqs. (21), as suggested by the numerical values obtained from the fits performed in Ref. [34], and $T'_{I_t=1}(0)$ and $T_{I_t=2}(0)$ are approximated by the lowest-order result in ChPT, see Eq. (52) below, the so-called Adler and σ sum rules (see e.g. [31] for a discussion based on current algebra and PCAC) are obtained,

$$
\frac{1}{f_\pi^2} = \frac{2}{\pi} \int_{2m_\pi^2}^{\infty} \frac{d\nu}{\nu} \sqrt{1 - \frac{4m_\pi^4}{\nu^2}} \left[\frac{1}{3}\sigma_0(\nu) + \frac{1}{2}\sigma_1(\nu) - \frac{5}{6}\sigma_2(\nu)\right], \tag{23}
$$

$$
\frac{m_\pi^2}{f_\pi^2} = \frac{2}{\pi} \int_{2m_\pi^2}^{\infty} d\nu \sqrt{1 - \frac{4m_\pi^4}{\nu^2}} \left[\frac{1}{3}\sigma_0(\nu) - \frac{1}{2}\sigma_1(\nu) + \frac{1}{6}\sigma_2(\nu)\right], \tag{24}
$$

with $f_\pi \sim 93$ MeV, the pion decay constant. Using the GKPRY parameterizations [34], one finds that the contribution of the region $\nu > 1.42$ GeV, for which Regge behavior is assumed, is quite small. This is because $\sigma_{I_t}(\nu) \to 4\pi^2 \beta_{I_t}(0) \nu^{\alpha_{I_t}(0)-1}$. In addition, we would like to point out

- $I_t = 1$: Following the discussion of the previous section, neglecting the contribution to the sum rule arising from the region $\sqrt{\nu} \in (1, 1.4)$ GeV might induce variations of order 20%, which we expect to be of the same order as those stemming from $\mathcal{O}(p^4)$ ChPT terms neglected in the left-hand side of the sum rule.

 The Adler sum rule is satisfied to 5% (see also [37]) in the partial-wave plus Regge representation.

- $I_t = 2$: This sum rule converges if $\alpha_{I_t=2}(0) < 0$ and is the σ sum rule derived in [31] on the basis of PCAC. The σ sum rule is already approximately satisfied for an upper limit of the integration around $\sqrt{s} < 1.26$ GeV. The contribution above this upper limit tends to cancel and shows an oscillating behavior as a function of the upper limit of the integration. This is closely linked with having a value of b_2 compatible with zero and a not well-defined sign for the ratio b_2/a_2 appearing in $R_{I_t=2}$. For an upper limit of $\sqrt{s} < 1.26$, the truncated Adler sum rule also provides a rather reasonable value of 89 MeV for f_π. This result is certainly more reasonable if one bears in mind that the left-hand side of the sum rule has been computed at lowest order in ChPT only. This observation suggests a kind of super-convergent dispersion relation which will be important to set up our model below.

[5] We use the UFD parameterization of Ref. [34].

Given the above discussion, one finds reasons to saturate the sum rules with the lowest-lying resonances below 1 GeV. In addition, we already mentioned that the $I_t = 0$ sum rule in Eq. (21) is saturated also, with great accuracy, at 1 GeV (integral and R contributions tend to cancel above 1 GeV). All this, gives support to the scenarios that will be presented below, in which we will take into account only the lowest-lying resonance degrees of freedom. Yet, we will make use of the Adler and σ sum rules, saturated at energies of about 1 GeV, to find out short-distance constraints that will make more predictive the RχT approach adopted here.

III. LARGE–N_C ASPECTS OF $\pi\pi$ SCATTERING

In this section we discuss some aspects of the large–N_C limit which will provide some useful guidance in our analysis of $\pi\pi$ scattering.

A. $\pi\pi$ elastic scattering amplitude in the SRA

From the lowest-order RχT Lagrangian [9, 10], describing the couplings of the lowest-lying $V(1^{--})$, $A(1^{++})$, $S(0^{++})$ and $P(0^{-+})$ resonance nonet multiplets to the pions, we find[6]

$$\begin{aligned} A^{\rm SRA}(s,t,u) &= \frac{m_\pi^2 - s}{f_\pi^2} + \frac{G_V^2}{f_\pi^4}\left\{\frac{t(s-u)}{t-m_V^2} + \frac{u(s-t)}{u-m_V^2}\right\} \\ &+ \frac{2}{3f_\pi^4}\frac{\left[c_d(s-2m_\pi^2)+2m_\pi^2\, c_m\right]^2}{s-m_{S_8}^2} \\ &+ \frac{4}{f_\pi^4}\frac{\left[\bar{c}_d(s-2m_\pi^2)+2m_\pi^2\, \bar{c}_m\right]^2}{s-m_{S_1}^2} \\ &+ \frac{8d_m^2}{f_\pi^4}\frac{m_\pi^4}{m_{P_8}^2 - m_\pi^2}\,. \end{aligned} \tag{25}$$

In the large–N_C limit, $|\bar{c}_d| = |c_d|/\sqrt{3}$ and $|\bar{c}_m| = |c_m|/\sqrt{3}$. We have specified for clarity the contributions from non-degenerate singlet, S_1, and iso-singlet octet, S_8, fields. Quite generally, $m_{S_8} - m_{S_1} = \mathcal{O}(1/N_C)$ and mixing effects have been analyzed in Refs. [38, 39].[7] Glueball mixing within RχT has been discussed in Ref. [40].

Taking $m_{S_8} = m_{S_1} = m_S$, $|\bar{c}_d| = |c_d|/\sqrt{3}$ and $|\bar{c}_m| = |c_m|/\sqrt{3}$, we reproduce the expressions in Ref. [41]. In principle, the couplings appearing in the scattering amplitude can be determined by analyzing the decay processes $\rho \to 2\pi$ and $S \to 2\pi$ with $S = \sqrt{2/3}S_1 + S_8/\sqrt{3}$, corresponding to a $(\bar{u}u + \bar{d}d)/\sqrt{2}$ flavor composition in the $q\bar{q}$ picture, which yield in the chiral limit (see also Ref. [42]),[8]

$$\Gamma_S = \frac{3c_d^2 m_S^3}{16\pi f_\pi^4}, \tag{26}$$

$$\Gamma_V = \frac{G_V^2 m_V^3}{48\pi f_\pi^4}. \tag{27}$$

[6] Here we use the antisymmetric field formulation where the A–π mixing is absent. Note that the axial resonance does not contribute to the elastic $\pi\pi$ scattering amplitude. After proper incorporation of short-distance constraints, the Proca formulation using $g_V = G_V/f_\pi$ yields the same amplitude [10]. $U(3)$ nonet resonance fields are generically parametrized as $R = \frac{1}{\sqrt{2}}\sum_{i=1}^{8} R_i\lambda_i + \frac{1}{\sqrt{3}}R_0$ with λ_i the standard Gell-Mann matrices.

[7] Ref. [39] finds sizeable mixing effects between the singlet and octet scalar-isoscalar mesons and identifies two possible phenomenologically acceptable scenarios for the tree-level mass eigenstates: a) $M_L = 1.35$ GeV and $M_H = 1.47$ GeV, or b) $M_L = 0.985$ GeV and $M_H = 1.74$ GeV. The light solution was less preferential at it would correspond to a case where $f_0(980)$ would not couple to pions. Therefore in several studies the heavy solution has been adopted.

[8] The full expressions are $\Gamma_S = \frac{3m_S^3}{16\pi f_\pi^4}\rho_S\left[c_d + (c_m - c_d)\frac{2m_\pi^2}{m_S^2}\right]^2$ and $\Gamma_V = \frac{G_V^2 m_V^3}{48\pi f_\pi^4}\rho_V^3$, where $\rho_R = \sqrt{1 - 4m_\pi^2/m_R^2}$.

The residues of the scalar-isoscalar and the vector-isovector poles in the partial-wave amplitudes are

$$\begin{aligned} g_S &= \frac{c_d m_S^2}{f_\pi^2}\,, \\ g_V &= \frac{G_V m_V^2}{\sqrt{3} f_\pi^2}\,. \end{aligned} \tag{28}$$

Note that the (large–N_C) relations $g_S^2 = 16\pi\Gamma_S m_S/3$ and $g_V^2 = 16\pi\Gamma_V m_V$ hold in the SRA, in the chiral limit. The SRA amplitude in Eq. (25) contains too many parameters to be analyzed in full detail. In the next subsections, we will discuss a sensible way of reducing the number of couplings and masses.

After projecting onto partial waves we get for the $(I,J) = (0,0)$, $(1,1)$ and $(2,0)$ channels the following asymptotic behavior at large values of s:

$$T_{IJ}^{\rm SRA}(s) = \lambda_{IJ}\,\frac{2c_d^2 + 3G_V^2 - f_\pi^2}{f_\pi^4}\,s + \ldots\,, \qquad \lambda_{00} = 1\,, \quad \lambda_{11} = \frac{1}{6}\,, \quad \lambda_{20} = -\frac{1}{2}\,. \tag{29}$$

The above behavior implies that subtractions would be necessary to make convergent a dispersion relation.[9] We will add subtraction constants *after* unitarization.

B. Short-distance constraints

The short-distance constraints encompass RχT with proper high-energy behavior [18]. In general they produce a set of conditions which, for a limited set of resonances and in particular in the SRA, reduce the number of independent couplings. These conditions may be over-determined yielding at times to mutually inconsistent values, a problem which can be side-stepped by introducing more resonances. In the present case we think it of interest to pursue such an analysis within $\pi\pi$ scattering.

In the chiral limit, the t-channel amplitudes, see Eq. (12), in the forward direction have the following asymptotic behavior in terms of the crossing-odd variable $\nu = (s-u)/2$:

$$\begin{aligned} T_{I_t=0}^{\rm SRA}(\nu,0) &= 2\,\frac{c_d^2 m_S^2 + \frac{2}{3} g_T^2 m_T^2 + G_V^2 m_V^2}{f_\pi^4} + \mathscr{O}(\nu^{-2})\,, \\ T_{I_t=1}^{\rm SRA}(\nu,0) &= \frac{6c_d^2 - 3f_\pi^2 + 4g_T^2 + 3G_V^2}{3f_\pi^4}\,\nu + \mathscr{O}(\nu^{-1})\,, \\ T_{I_t=2}^{\rm SRA}(\nu,0) &= 2\,\frac{c_d^2 m_S^2 + \frac{2}{3} g_T^2 m_T^2 - G_V^2 m_V^2/2}{f_\pi^4} + \mathscr{O}(\nu^{-2})\,, \end{aligned} \tag{30}$$

where we have included momentarily the tensor meson coupling g_T and mass m_T, to be discussed below in more detail. This limit is compatible with the Froissart bound, a specific merit of the antisymmetric tensor formulation [10].[10]

As already mentioned, it makes sense to divide the $\pi\pi$ scattering amplitudes in Eq. (13) into three pieces: i) the low-energy part which takes the form of subtraction constants and is fixed by chiral symmetry, ii) an intermediate-energy part, dominated by resonance exchange, and iii) the high-energy remainder which we expect to be responsible for the Regge behavior. Therefore, if we impose a behavior for the resonance contribution no worse than suggested by Regge theory, we obtain the constraints

$$f_\pi^2 = 2c_d^2 + \frac{4}{3} g_T^2 + G_V^2\,, \tag{31}$$

$$0 = 6c_d^2 m_S^2 + 4g_T^2 m_T^2 - 3G_V^2 m_V^2\,. \tag{32}$$

[9] Requiring that the leading term proportional to λ_{IJ} vanishes would yield the relation $2c_d^2 + 3G_V^2 = f_\pi^2$, advocated in Ref. [42]. This would imply $G_V \leq f_\pi/\sqrt{3}$, giving a 30% too small $\rho \to 2\pi$ decay width. This relation has also been found as a necessary high-energy constraint in a NLO RχT analysis of the vector form factor, incorporating subleading $1/N_C$ corrections [43]. In the $c_d = 0$ limit, it gives $G_V = f_\pi/\sqrt{3}$, which was also found in the study of one-meson radiative tau decays carried out in [44]. Notice however that imposing this relation is not enough to make subtractions unnecessary, because the partial waves would still grow at large values of s as $T_{IJ}(s) \sim (m_V^2 G_V^2/f_\pi^4)\log(s/m_V^2)$.

[10] Physical results are actually independent of the field representation. The naive exchange of Proca fields does not satisfy the Froissart bound, but after suitable polynomial subtractions to comply with the short-distance constraints, one ends up with the same amplitude [10]. Fields remain a useful framework to incorporate symmetries, see also the discussion in Ref. [45].

These constraints correspond to require that the ν and the ν^0 coefficients of $T^{\rm SRA}_{I_t=1}$ and $T^{\rm SRA}_{I_t=2}$, respectively, vanish in the large–ν regime. The second condition is less robust than the first one, attending to what we have discussed on Regge phenomenology above. Indeed, Eqs. (31) and (32) can be also obtained from the Adler and σ sum rules, in the chiral limit, using the narrow resonance approximation of Eq. (11) to estimate the cross sections that appear in the right-hand sides of the sum rules. Note, that since we have not considered any exotic isotensor resonance, we are approximating $\sigma_2 = 0$.

In the absence of tensor couplings, $g_T = 0$, these constraints imply $c_d = \sin\phi\, f_\pi/\sqrt{2}$, $G_V = \cos\phi\, f_\pi$ and $m_V/m_S = \tan\phi$, where ϕ is a mixing angle. The KSFR relation ($G_V = f_\pi/\sqrt{2}$) requires $\phi = \pi/4$ and hence $m_S = m_V$, as well as $2c_d = \sqrt{2}G_V = f_\pi$, implying $\Gamma_S = 9\Gamma_V/2$. These constraints have also been found in the algebraic chiral-symmetry approach [46–48] and can be re-written, in terms of the decay widths, as

$$1 \;=\; \frac{\Gamma_S}{m_S}\frac{32\pi f_\pi^2}{3m_S^2} + \frac{9}{2}\frac{\Gamma_V}{m_V}\frac{32\pi f_\pi^2}{3m_V^2}\,, \tag{33}$$

$$0 \;=\; \frac{\Gamma_S}{m_S} - \frac{9}{2}\frac{\Gamma_V}{m_V}\,, \tag{34}$$

which yield the value of the scalar mass and width to be

$$m_S = 660\ {\rm MeV}\,, \qquad \Gamma_S = 570\ {\rm MeV}\,, \tag{35}$$

when phenomenological values for the mass and width of the ρ meson are used. These numbers are quite sensitive to details. For instance if the KSFR set of parameters is used, one gets instead (taking as input the ρ meson mass)

$$m_S = m_V = 775\ {\rm MeV}\,, \qquad \Gamma_S = \frac{9}{2}\Gamma_V = 805\ {\rm MeV}\,. \tag{36}$$

Of course, given the fact that the scalar turns out to be a broad resonance, it is unclear what these estimates should be compared to, since generally a resonance is characterized by the complex pole and the complex residue of the scattering amplitude. The benchmark calculation of the pole on the second Riemann sheet of the $\pi\pi$ scattering amplitude [2, 3], when written as $s_\sigma = m_\sigma^2 - {\rm i}m_\sigma\Gamma_\sigma$, yields $m_\sigma = 347(17)$ MeV and $\Gamma_\sigma = 690(48)$ MeV. On the other hand, the connection between the Breit-Wigner (BW) resonance parameters, defined as $\delta(m^2_{\rm BW}) = \pi/2$ and $\Gamma_{\rm BW} = 1/(m_{\rm BW}\delta'(m^2_{\rm BW}))$, and the pole resonance parameters has been discussed on the light of their N_C behavior in a model-independent fashion [19], suggesting that the large shift in the mass is $\mathcal{O}(1/N_C^2)$ and can be computed, yielding an acceptable extrapolation of $m_{\rm BW} \sim 700$ MeV. The recent $\pi\pi$–scattering analysis of Ref. [34] leads to the Breit-Wigner values $[m_{\sigma,\,\rm BW}, \Gamma_{\sigma,\,\rm BW}] = [841(5)\ {\rm MeV}, 820(20)\ {\rm MeV}]$.[11] The quoted errors above also account for the existing differences when UFD and CFD parameterizations are used. This yields a ratio $\Gamma_{\sigma,\,\rm BW}/m_{\sigma,\,\rm BW} \sim 5.0(1)\ \Gamma_{\rho,\,\rm BW}/m_{\rho,\,\rm BW}$, which suggests a 10% accuracy of large N_C in the SRA, supporting as well the identification of the large–N_C parameters with the BW ones.

C. Higher-energy resonances

We have so far been limited to states below the $\bar{K}K$ threshold, $\sqrt{s} < 1$ GeV. On the other hand, Regge behavior works for $\sqrt{s} > 1.4$ GeV. So, it is interesting to see the modifications induced by other resonances which may decay into 2π, in the mass range 1 GeV $< m_R <$ 1.4 GeV, namely $f_0(980)$, $h_1(1170)$, $b_1(1235)$, $f_2(1275)$, $f_0(1370)$ and $\rho_1(1450)$.

After implementing the appropriate short-distance constraints, via the Froissart bound, the inclusion of a 2^{++} tensor yields a resonance amplitude [49]

$$A_T(s,t,u) = -\frac{2g_T^2}{f_\pi^4}\,\frac{(t-u)^2 - s^2/3}{m_T^2 - s} - \frac{4g_T^2}{f_\pi^4}\,\frac{(s^2 - t^2 - u^2)}{m_T^2}\,, \tag{37}$$

where the coupling is determined from the decay into $\pi\pi$ in a relative D-wave yielding

$$\Gamma_T = \frac{g_T^2 m_T^3}{40\pi f_\pi^4}\,\rho_T^5\,. \tag{38}$$

[11] The value of the pole is $\sqrt{s_\sigma} = 445(8) - {\rm i}297(7)$ MeV, in agreement with Ref. [2]. On the other hand, the model-independent large–N_C-based extrapolation from the resonance pole mass to the BW pole mass [19] yields $m_{\sigma,\,\rm BW} = 670(20)$ MeV, when the UFD parameterization of Ref. [34] is used.

The previous amplitude yields the following contributions to the $\mathcal{O}(p^4)$ ChPT couplings [49]: $L_1^T = L_2^T = 0$ and $L_3^T = g_T^2/(3m_T^2) \sim 0.16\times 10^{-3}$ (see also Ref. [50]). The axial 1^{+-} mesons, such as $h_1(1170)$ and $b_1(1235)$, give just a purely polynomial contribution to the $\pi\pi$ scattering amplitude (without s-channel propagator poles) which cannot satisfy the Froissart bound, yielding to no contribution at all to the LECs. We remind that the exchange of $J>1$ resonances in the t-channel naively violates the Froissart bound, a situation which has been the standard motivation to rely on high-energy Regge behavior as a way of introducing suitable cancellations.

If the tensor meson $f_2(1275)$ is considered, we might include $\rho' \equiv \rho_1(1450)$ and $f_0(980)$ as well, where the decay widths into $\pi\pi$ are taken to be $\Gamma(f_2\to\pi\pi) = 150$ MeV, $\Gamma(f_0\to\pi\pi) = 80$ MeV and $\Gamma(\rho'\to\pi\pi) = 250$ MeV (note the large inaccuracies). This yields the extended sum rules (we remain in the chiral limit)

$$\begin{aligned} 1 &= \sum_S \frac{\Gamma_S}{m_S}\frac{32\pi f_\pi^2}{3m_S^2} + \sum_V \frac{9}{2}\frac{\Gamma_V}{m_V}\frac{32\pi f_\pi^2}{3m_V^2} + \sum_T 5\frac{\Gamma_T}{m_T}\frac{32\pi f_\pi^2}{3m_T^2}\,, \\ 0 &= \sum_S \frac{\Gamma_S}{m_S} + \sum_T 5\frac{\Gamma_T}{m_T} - \sum_V \frac{9}{2}\frac{\Gamma_V}{m_V}\,. \end{aligned} \tag{39}$$

Using PDG values [51], the higher resonances $f_0(980)$, $f_2(1275)$ and $\rho_1(1450)$ produce corrections of the order of $(0.06, -0.01)$ for the r.h.s of the first and second sum rules respectively. This shows a trend to cancellation which supports that higher states not only play a minor role at low energies but also in the region of interest below 1 GeV, to leading order in N_C. Therefore we will carry our analysis below with just scalar 0^{++} and vector 1^{--} states.[12]

D. Other short-distance constraints

Alternatively to the previous analysis, one may derive short-distance constraints from other processes involving two- and three-point functions [10, 14]. Imposing the short-distance properties of the underlying QCD dynamics, within the SRA, one gets [9, 18]:

$$\sqrt{2}G_V = 2c_d = 2c_m = 2\sqrt{3}\,\bar{c}_d = 2\sqrt{3}\,\bar{c}_m = 2\sqrt{2}d_m = f_\pi\,. \tag{40}$$

These constraints are obtained from a variety of processes, some of them involving electroweak probes. It is remarkable that they turn out to be totally compatible with those deduced here by looking to $\pi\pi$ phenomenology at high energies, for a vanishing tensor-meson contribution ($g_T = 0$). Neglecting the $f_2(1270)$ and higher-mass resonance contributions leads to a realistic and simplified scenario for the purpose of the present work. On the other hand, from the $\pi\pi$ scattering amplitude, we have derived the additional restriction $m_S = m_V$. Although we will explore the effects of this constraint in one of the fits that will be presented below, we should mention here that it relies on the assumption of an asymptotic behavior for $T_{I_t=2}(\nu)$ more convergent than that of a constant (ν^0). This is not a totally robust result, though it is certainly plausible, given the accuracy of current $\pi\pi$ analyses at high energies [34].

For $m_V = 775$ MeV, the conditions in Eq. (40) lead to

$$\Gamma_S = \frac{3m_S^3}{64\pi f_\pi^2}\,\rho_S = 750\ \text{MeV}\,, \tag{41}$$

$$\Gamma_V = \frac{m_V^3}{96\pi f_\pi^2}\,\rho_V^3 = 150\ \text{MeV}\,. \tag{42}$$

Besides, by requiring the two-point correlation functions of two scalar or two pseudoscalar currents to be equal at high energies, up to corrections of the order $\alpha_s f^4/t^2$, one finds [18] $m_{P_8} = \sqrt{2}m_S$. This relation involves a small correction, of the order 5%, which we neglect, together with the tiny effects from light quark masses. We will use Eq. (40) to fix our parameters below, but allowing m_S to be different from m_V.

[12] Of course, it is intriguing to analyze the role of the $(I^G, J^{PC}) = (2^+, 0^{++})$ exotic state, named X(1420) in the PDG [51] (and found also in the SU(6) study of Ref. [52]), which decays into 2π in a S wave with estimated mass $M_X = 1420(20)$ MeV and width $\Gamma_X = 160(20)$ MeV. The contributions of such a state to the Adler and σ sum rules, Eqs. (23,24), in the narrow-resonance approximation are $-80\pi\Gamma_X/3m_X^3 \sim -4.6\ \text{GeV}^{-2}$ and $16\pi\Gamma_X/3m_X \sim 1.9$, respectively. As compared to the individual contributions from other mesons, they seem too small to provide a clear signal.

IV. ONE-LOOP CHPT CORRECTIONS AND UNITARIZATION OF THE $\pi\pi$ ELASTIC SCATTERING AMPLITUDE

A. $\pi\pi$ scattering at one loop in ChPT

At $\mathcal{O}(p^4)$ in ChPT, the $\pi\pi$ elastic scattering amplitudes can be written in the form [12]:

$$A^{\rm ChPT}(s,t,u) = A_2^{\rm ChPT}(s,t,u)+A_4^{\rm ChPT}(s,t,u), \tag{43}$$

$$A_2^{\rm ChPT}(s,t,u) = \frac{m_\pi^2-s}{f_\pi^2}, \tag{44}$$

$$\begin{aligned} A_4^{\rm ChPT}(s,t,u) &= \frac{-1}{96\pi^2 f_\pi^4}\Big\{(2\bar{l}_1+\bar{l}_2-\frac{7}{2})s^2+(\bar{l}_2-\frac{5}{6})(t-u)^2+4(3\bar{l}_4-2\bar{l}_1-\frac{1}{3})m_\pi^2 s-(3\bar{l}_3+12\bar{l}_4-8\bar{l}_1-\frac{13}{3})m_\pi^4 \\ &+ 3(s^2-m_\pi^4)\bar{J}(s)+\big(t(t-u)-2m_\pi^2 t+4m_\pi^2 u-2m_\pi^4\big)\bar{J}(t)+\big(u(u-t)-2m_\pi^2 u+4m_\pi^2 t-2m_\pi^4\big)\bar{J}(u)\Big\}. \end{aligned} \tag{45}$$

The lowest-order amplitude $A_2^{\rm ChPT}(s,t,u)$ is identical to the first term in Eq. (25) (pion contribution) and only depends on the pion mass and weak decay constant. The $\mathcal{O}(p^4)$ correction involves four SU(2) renormalization-scale-independent LECs: $\bar{l}_i$ ($i=1,2,3,4$). In addition, $A_4^{\rm ChPT}(s,t,u)$ includes one-loop chiral corrections, which are suppressed by one power of $1/N_C$; they are parameterized through the loop function

$$\bar{J}(s) = 2+\rho(s)\log\left[\frac{\rho(s)-1}{\rho(s)+1}\right]. \tag{46}$$

For the sake of completeness, we recall here, the relation between the LECs $\bar{l}_i$ and the most common SU(3) parameters $L_i^r(\mu)$ [12, 13]:

$$\bar{l}_i = \frac{32\pi^2}{\gamma_i}l_i^r(\mu)-\log(m_\pi^2/\mu^2), \tag{47}$$

where

$$\gamma_1=\frac{1}{3},\quad \gamma_2=\frac{2}{3},\quad \gamma_3=-\frac{1}{2},\quad \gamma_4=2 \tag{48}$$

and

$$\begin{aligned} l_1^r &= 4L_1^r+2L_3-\frac{\nu_K}{24}, \\ l_2^r &= 4L_2^r-\frac{\nu_K}{12}, \\ l_3^r &= -8L_4^r-4L_5^r+16L_6^r+8L_8^r-\frac{\nu_\eta}{18}, \\ l_4^r &= 8L_4^r+4L_5^r-\frac{\nu_K}{2}, \end{aligned} \tag{49}$$

with $32\pi^2\nu_{K,\eta}=1+\log(\hat{m}_{K,\eta}^2/\mu^2)$, $\hat{m}_\eta=4\hat{m}_K/3$ and $\hat{m}_K\sim 468$ MeV the kaon mass in the limit $m_u=m_d=0$. The renormalized coupling constants $l_i^r(\mu)$ and $L_i^r(\mu)$ depend logarithmically on the dimensional regularization scale μ:

$$L_i^r(\mu_2)=L_i^r(\mu_1)+\frac{\Gamma_i}{16\pi^2}\log(\frac{\mu_1}{\mu_2}), \tag{50}$$

where

$$\Gamma_1=\frac{3}{32},\quad \Gamma_2=\frac{3}{16},\quad \Gamma_3=0,\quad \Gamma_4=\frac{1}{8},\quad \Gamma_5=\frac{3}{8},\quad \Gamma_6=\frac{11}{144},\quad \Gamma_8=\frac{5}{48}. \tag{51}$$

The corresponding t-channel forward scattering amplitudes at $\nu=0$ are given by:

$$\begin{aligned} T_{I_t=0}(0) &= \frac{m_\pi^2}{2f_\pi^2}+\frac{m_\pi^4(-72\bar{l}_1-48\bar{l}_2+45\bar{l}_3+36\bar{l}_4+39\pi-101)}{576\pi^2 f_\pi^4}+\mathcal{O}(p^6), \\ T'_{I_t=1}(0) &= -\frac{1}{f_\pi^2}+\frac{(-48\bar{l}_4+9\pi-10)m_\pi^2}{384\pi^2 f_\pi^4}+\mathcal{O}(p^6), \\ T_{I_t=2}(0) &= -\frac{m_\pi^2}{f_\pi^2}+\frac{(-48\bar{l}_2+18\bar{l}_3-72\bar{l}_4+21\pi+10)m_\pi^4}{576\pi^2 f_\pi^4}+\mathcal{O}(p^6). \end{aligned} \tag{52}$$

The $\mathcal{O}(p^4)$ corrections are at the $10-20\%$ level of the lowest-order ones in the Adler and σ sum rules.

B. $\mathcal{O}(p^4)$ ChPT-improved SRA amplitudes and large–N_C counting rules.

In the limit of a large number of colors [7, 8], $A^{\rm SRA}$ in Eq. (25) scales like $1/N_C$, since the pion weak decay constant behaves like $\mathcal{O}(\sqrt{N_C})$. Furthermore, $A^{\rm SRA}$ provides the leading–N_C prediction for the actual $\pi\pi$ scattering amplitude, with the only limitation of considering just the lowest-lying nonet of exchanged resonances [9]. This latter approximation is justified as long as s, t and u are kept far from the second resonance region.

The lightest resonances have an important impact on the low-energy dynamics of the pseudoscalar bosons. Below the resonance mass scale, the singularity associated with the pole of a resonance propagator is replaced by the corresponding momentum expansion; therefore, the exchange of virtual resonances generates derivative Goldstone couplings proportional to powers of $1/m_R^2$. At lowest order in derivatives, this gives the large–N_C predictions for the $\mathcal{O}(p^4)$ ChPT couplings [9]. At $\mathcal{O}(p^4)$ the amplitude $A^{\rm SRA}$ in Eq. (25) reduces to

$$\begin{aligned} A_4^{\rm SRA}(s,t,u) &= \frac{m_\pi^2-s}{f_\pi^2} - \frac{G_V^2}{f_\pi^4}\left\{\frac{t(s-u)}{m_V^2}+\frac{u(s-t)}{m_V^2}\right\} \\ &- \frac{2}{3f_\pi^4}\frac{\left[c_d(s-2m_\pi^2)+2m_\pi^2\, c_m\right]^2}{m_{S_8}^2} \\ &- \frac{4}{f_\pi^4}\frac{\left[\bar{c}_d(s-2m_\pi^2)+2m_\pi^2\, \bar{c}_m\right]^2}{m_{S_1}^2} \\ &+ \frac{8d_m^2}{f_\pi^4}\frac{m_\pi^4}{m_{P_8}^2}\,, \end{aligned} \tag{53}$$

which constitutes the leading $1/N_C$ approximation to $A^{\rm ChPT}$. The polynomial form can be re-written as

$$\begin{aligned} A_4^{\rm SRA}(s,t,u) &= \frac{m_\pi^2-s}{f_\pi^2} - \frac{4}{f_\pi^4}\left\{(2L_1^{\rm SRA}+L_3^{\rm SRA})(s-2m_\pi^2)^2 + L_2^{\rm SRA}\left[(t-2m_\pi^2)^2+(u-2m_\pi^2)^2\right]\right\} \\ &- \frac{8m_\pi^2}{f_\pi^4}\left\{(2L_4^{\rm SRA}+L_5^{\rm SRA})s + (4L_6^{\rm SRA}+2L_8^{\rm SRA}-4L_4^{\rm SRA}-2L_5^{\rm SRA})m_\pi^2\right\}. \end{aligned} \tag{54}$$

From Eqs. (53) and (40), one trivially finds

$$\begin{aligned} &2L_1^{\rm SRA} = L_2^{\rm SRA} = \frac{f_\pi^2}{8m_V^2}\,, \quad L_3^{\rm SRA} = -\frac{3f_\pi^2}{8m_V^2}+\frac{f_\pi^2}{8m_S^2}\,, \\ &L_4^{\rm SRA} = 0\,, \quad L_5^{\rm SRA} = \frac{f_\pi^2}{4m_S^2}\,, \quad L_6^{\rm SRA} = 0\,, \quad L_8^{\rm SRA} = \frac{3f_\pi^2}{32m_S^2}\,, \end{aligned} \tag{55}$$

in full agreement with Ref. [18].[13]

Let us pay now some attention to the N_C dependence of the one-loop ChPT amplitude. Note that from Eq. (45), the logarithmic contribution to $A_4^{\rm ChPT}$ scales as $1/N_C^2$, while the polynomial piece behaves as $1/N_C$ in the $N_C \gg 1$ limit. This is because, as shown in the relations (55), the LECs L_i behave as $\mathcal{O}(N_C)$, with the exceptions of L_2-2L_1, L_4 and L_6 that scale as $\mathcal{O}(N_C^0)$ [13]. The renormalization scale dependence of the LECs provides further subleading contributions in the $1/N_C$ counting. Unfortunately, the measured values of the L_i couplings cannot be phenomenologically split into their large–N_C leading and subleading parts. In general, one has the scale-dependent relation

$$L_i^r(\mu) = A_i N_C + B_i(\mu)\,, \tag{56}$$

where A_i is scale independent. Note that only the $N_C = 3$ combination is experimentally accessible. However a meaningful extension of the chiral amplitudes to an arbitrary number of colors requires some knowledge of the coefficients A_i and B_i. This

[13] If the relation $m_S = m_V$ is further assumed, one gets purely geometrical ratios for the non-vanishing LECs:

$$2L_1^{\rm SRA} = L_2^{\rm SRA} = -\frac{1}{2}L_3^{\rm SRA} = \frac{1}{2}L_5^{\rm SRA} = \frac{4}{3}L_8^{\rm SRA} = \frac{f_\pi^2}{8m_V^2}\,.$$

In chiral quark models with meson dominance built-in one also has $m_S = m_V = \sqrt{24/N_C}\pi f \sim 781$ MeV, for $f = 88$ MeV [53], so that the above relations hold with $L_2 = N_C/192\pi^2 = 1.5\times 10^{-3}$.

difficulty is precisely what $A_4^{\rm SRA}$ helps to overcome, and thus the SRA predictions of Eq. (55) can be used to read off the A_i coefficients.[14]

In the recent work of Ref. [29], the SRA parameters G_V, c_d, c_m, $\overline{c}_d$, $\overline{c}_m$, m_V, m_{S_8} and m_{S_1} are fitted to data. Afterwards and to extrapolate to $N_C > 3$, the resonance masses are kept constant, while all the couplings are scaled by a $\sqrt{N_C/3}$ factor. This does not take into account that singlet and octet scalar resonances become degenerate in the large–N_C limit. On the other hand, if one fits the resonance couplings to data, the fitted values do not necessarily match their leading–N_C values in Eq. (40) and might incorporate some significant $1/N_C$ subleading contributions, which later on however, are scaled as if they were leading in the N_C counting. For instance, in Ref. [29] a value of around 15 MeV is found for c_d, which is around a factor three smaller than that of $f_\pi/2$ quoted in Eq. (40). A proper extension of this parameter when N_C deviates from 3 should be $2c_d = f_\pi^{N_C=3} \times \sqrt{N_C/3} + (30\ {\rm MeV} - f_\pi^{N_C=3})$, instead of that assumed in [29]. For other parameters, there exist also large deviations between the fitted values found in [29] and the leading–N_C estimates given in Eq. (40). These differences seem to indicate $1/N_C$ corrections to the resonance parameters which are much larger than expected. One might wonder the underlying origin of these disturbing large deviations. The fitting strategy certainly might play some role on this; for instance, the choice of the upper energy limit or the choice of the unitarization procedure. This latter issue has some relevance which we will address now. In the next section, we will discuss our unitarization procedure, which is rather similar to that used in Ref. [29]. There appear independent subtraction constants for each of the $(I,J) = (0,0)$, $(1,1)$ and $(2,0)$ sectors [33, 54]. However, in Ref. [29], all three subtraction constants were forced to be equal. From the discussion in [33, 54], this is somehow an arbitrary choice. The lack of flexibility of data fits incorporating such constraint might influence the actual values determined for the resonance couplings and their estimated scaling with N_C.

Let us come back to our scheme. The amplitude $A_4^{\rm SRA}$ in Eq. (54) contains neither pion loop terms, nor the $1/N_C$ subleading contributions to the polynomial piece of the one-loop ChPT amplitude. Thus, and to better describe the experimental phase shifts for $N_C = 3$, we propose to use

$$A^{SRA+{\rm ChPT}}(s,t,u) \;=\; \underbrace{A^{\rm SRA}(s,t,u)}_{\mathcal{O}(1/N_C)} + \underbrace{\left[A^{\rm ChPT}(s,t,u) - A_4^{\rm SRA}(s,t,u)\right]}_{\mathcal{O}(1/N_C^2)} . \tag{57}$$

In this way, by construction, we recover the one-loop ChPT results, while at the same time, all terms in the amplitude that scale like $1/N_C$ (leading) are also included, within the SRA. Note, that in the $1/N_C$ counting, the correction $\left\{A^{\rm ChPT}(s,t,u) - A_4^{\rm SRA}(s,t,u)\right\}$ is incomplete, since it does not account for all existing subleading $1/N_C^2$ contributions to $A(s,t,u)$. A complete $1/N_C^2$ calculation would require quantum corrections stemming also from the low-lying resonances [43, 55–59].

C. Unitarized amplitudes

The ChPT loops incorporate the unitarity field theory constraints in a perturbative manner, order by order in the chiral expansion. Though subleading in the $1/N_C$ counting, their effect appears to be crucial for a correct understanding of S-wave $\pi\pi$ phase shifts. Furthermore, resonances show up as poles of the unitarized amplitudes in unphysical sheets, which positions provide their masses and widths. Thus, to discuss the nature of the $f_0(600)$ resonance, it is crucial to restore unitarity. Any unitarization method re-sums a perturbative expansion of the scattering amplitude in such a way that two-body elastic unitarity,

$$ {\rm Im} T_{IJ}^{-1}(s) = \frac{\rho(s)}{16\pi}, \qquad s > 4m_\pi^2, \tag{58}$$

is implemented exactly. To restore unitarity, we will make use here of a once-subtracted dispersive representation of $T_{IJ}^{-1}(s)$ (see for instance Sect. 6 of Ref. [33]). Let be $\mathscr{T}_{IJ}^{SRA+{\rm ChPT}}(s)$ and $[T_2]_{IJ}(s)$, the $\pi\pi$ amplitudes, in the (I,J) sector, deduced from $A^{SRA+{\rm ChPT}}(s,t,u)$ and $A_2^{\rm ChPT}(s,t,u)$, respectively. We define an unitarized amplitude as [33]

$$T_{IJ}^{-1}(s) \;=\; -C_{IJ} - \overline{I}_0(s) + V_{IJ}^{-1}(s)\,, \tag{59}$$

$$V_{IJ}(s) \;=\; \mathscr{T}_{IJ}^{SRA+{\rm ChPT}}(s) - [T_2]_{IJ}(s)\,(\overline{I}_0(s) + C_{IJ})\,[T_2]_{IJ}(s)\,, \tag{60}$$

where V_{IJ} stands for the two-particle irreducible amplitude, and the subtraction constant and the loop function are given by

$$C_{IJ} = -T_{IJ}^{-1}(4m_\pi^2) + V_{IJ}^{-1}(4m_\pi^2), \qquad \overline{I}_0(s) = \frac{1}{16\pi^2}\left[2 - \overline{J}(s)\right]. \tag{61}$$

[14] Actually, the SU(2) scale-independent LECs defined by Eq. (47) display the N_C separation in a scale-independent fashion, since $\overline{l}_i = a_i N_C + b$ where b is *common* to all coefficients and stems from pion loops. This allows to build differences, $\overline{l}_i - \overline{l}_j = (a_i - a_j)N_C$, which can be used to extract the leading–N_C contributions from data up to a constant. This is illustrated in quark model calculations [53].

Note that *i)* the constants C_{IJ} determine the scattering length/volume in each sector and become undetermined free parameters, and *ii)* with the election of $V_{IJ}^{-1}(s)$, and considering $A^{\rm SRA}(s,t,u)-A_4^{\rm SRA}(s,t,u)$ as $\mathcal{O}(p^6)$, we recover from $T_{IJ}(s)$ the ChPT series up to one loop, in all (I,J) sectors.

Analytical expressions for the ChPT amplitudes projected onto the different (I,J) sectors can be found in the appendix B of Ref. [33].

A final remark concerning the $1/N_C$ counting rules is in order here. The subtraction constants C_{IJ} must scale as

$$C_{IJ}\sim\mathcal{O}(N_C^0)\,, \tag{62}$$

because of their definition as the difference between the inverses of the full and the two-particle-irreducible amplitudes at threshold for each (I,J) sector.[15] Thus, the amplitude $T_{IJ}(s)$ reduces to the $1/N_C$ leading part of $\mathcal{T}_{IJ}^{SRA+{\rm ChPT}}(s)$ in the limit of a large number of colors.

V. $N_C = 3$ PHASE SHIFTS AND ρ AND $f_0(600)$ MESON PROPERTIES.

In this section, we fit the C_{IJ} parameters to phase-shift data and show results for the poles found in the second Riemann sheet (SRS) of the amplitudes. The SRS of the T matrix is determined by the definition of the loop function $\bar{I}_0(s)$ in the SRS. We follow here Ref. [60] and use Eq. (A13) of this latter reference to compute $\bar{I}_0(s)$ in the SRS.[16]

Masses and widths of the dynamically generated resonances are determined from the positions of the poles, s_R, in the SRS of the corresponding scattering amplitudes in the complex s plane, namely $s_R = M_R^2 - {\rm i}\, M_R\Gamma_R$. For narrow resonances ($\Gamma_R \ll M_R$), $\sqrt{s_R}\sim M_R - {\rm i}\Gamma_R/2$ constitutes a good approximation.[17]

The coupling constants of each resonance to the pion pair are obtained from the residues at the pole, by matching the amplitudes to the expression

$$T_{SRS}^{IJ}(s) = \frac{g_R^2}{(s-s_R)}\,, \tag{63}$$

for values of s close to the pole. The couplings g_R are complex in general, and represent independent information from the pole s_R. In the narrow-resonance approximation, the extrapolation of Eq. (63) to the real axis takes a Breit-Wigner form to comply with unitarity and hence $g_R^2 = 16\pi m_R\Gamma_R/\rho(m_R^2)$.

The first issue is to select the set of data points to be fitted. We will consider the scalar–isoscalar, vector–isovector and scalar–isotensor elastic $\pi\pi$ phase shifts, with a total of 107 data points, as follows.

- $I=J=0$ sector: As our main input, we will use the Roy-equations results from Refs. [3, 61, 62] in the energy range $\sqrt{s}\leq 750$ MeV. We take this upper c.m. energy cut to keep negligible coupled-channel $K\bar{K}$ effects, which give rise to the $f_0(980)$ resonance. We have considered the phase-shift determinations of Ref. [61] and that of Eq. (4.8) of Ref. [62]. For each value of $\sqrt{s}$, we have used as central value the average of both results, while the absolute difference between them is taken as the error for the χ^2 fit. From threshold to the upper cut of 750 MeV, we have moved up in steps of 10 MeV, which amounts to a total of 48 phase shifts to be fitted.

- $I=J=1$ ($I=2, J=0$) sector: We fit to the phase shifts compiled in Refs. [63, 64] ([65, 66]) and consider an upper cut of $\sqrt{s}\leq 910$ MeV (1190 MeV), which comprises a total of 38 (21) phase shifts.

An important point has been the selection of the fitting interval. Clearly we should restrict the range to the elastic region and, in particular, below the opening of the first inelastic $K\bar{K}$ channel. At lowest order, this effect corresponds to the two-step process $\pi\pi\to K\bar{K}\to\pi\pi$, which in the sub-threshold region yields a real contribution to the amplitude and is $1/N_C^2$ and $s_{K\bar{K}}$–suppressed. The pure elastic re-scattering is just $1/N_C^2$–suppressed. On the other hand, corrections to the SRA due to heavier states with mass M are of $\mathcal{O}(1/(N_C M^2))$. Therefore we expect that, by restricting to low energies, inelastic effects can be safely included in $1/N_C$ corrections to the LECs. In other words, we may allow $M\sim 2M_K\sim 1$ GeV without much trouble.

[15] The full and the two-particle-irreducible amplitudes differ by terms which always contains at least one s-channel pion loop, which is subleading in the $1/N_C$ power counting. Thus, the difference $T^{-1}-V^{-1}$ scales as $\mathcal{O}(N_C^0)$, as one readily deduces by noting that both TV and $(T-V)$ scale as $\mathcal{O}(1/N_C^2)$ in the $N_C\gg 1$ limit.

[16] Note that the function $\bar{J}_0(s)$, defined in Eq. (A8) of [60], reduces to $\bar{I}_0(s)$ for equal masses.

[17] It has become customary to quote for the broad σ the number $\sqrt{s_\sigma}$ instead of s_σ. Here, we will also quote $\sqrt{s_\sigma}$, but we will refrain from identifying ${\rm Re}\sqrt{s_\sigma}$ with the mass and $-2{\rm Im}\sqrt{s_\sigma}$ with the width of the resonance. For the ρ meson, the narrow-resonance approximation works within two standard deviations.

The second issue is to design the fit procedure. For three out of the five fits examined here, we will fix

$$m_V = 0.77 \text{ GeV}, \qquad m_S = 1 \text{ GeV}. \tag{64}$$

For the fit **B.3**, we will force $m_V = m_S$, as suggested from our discussion of Eqs. (31) and (32), and fit the common value to data. Finally, in the fit **B.1-2** we will fix m_V to 0.77 GeV, while m_S is considered as a free parameter. We will always fit C_{00}, C_{11} and C_{20} to data; besides those parameters, m_V and $m_S = m_P/\sqrt{2}$, $A^{SRA+\text{ChPT}}$ depends still on $L^r_{1,2,3,4,5,6,8}(\mu)$, once the relations in Eq. (40) are implemented.

We have considered two well-differentiated scenarios:

- **A**: We just take the SU(3) Gasser-Leutwyler parameters $L_i^r(\mu)$, at a certain scale μ, from other phenomenological analyses. In this type of fits, only the C_{IJ} parameters are fitted to data.

- **B**: The contributions of the low-lying vector, axial–vector, scalar and pseudoscalar resonances to the L_i, and therefore to the effective chiral Lagrangian at order $\mathcal{O}(p^4)$, were given in Eq. (55), and thus, the renormalized coupling constants $L_i^r(\mu)$ can be written as a sum [9]

$$L_i^r(\mu) = L_i^{\text{SRA}} + \hat{L}_i^r(\mu) \tag{65}$$

of the resonance contributions, L_i^{SRA} and a remainder $\hat{L}_i^r(\mu)$. The choice of the renormalization scale μ is arbitrary. However, it is rather obvious that one can only expect the resonances to dominate the $L_i^r(\mu)$ when μ is not too far away from the resonance region. Therefore, it is common to adopt $\mu = m_\rho$ as a reasonable choice. However, one might take as a best fit parameter one scale, μ^{RS}, for which it occurs a complete resonance saturation of all the LECs L_i^r, this is to say,

$$\hat{L}_i^r(\mu^{RS}) = 0\,. \tag{66}$$

In other words, at this privileged scale μ^{RS}, there is no other contribution in addition to the meson resonances. In this type of fits, besides the C_{IJ} parameters, this scale should be fitted to data.

We have also considered a scenario where the complete resonance saturation of the LECs L_i^r occurs at two different scales, μ_V^{RS} for $L^r_{1,2}$ and μ_S^{RS} for $L^r_{4,5,6,8}$, depending whether the LEC is dominated by the vector or the scalar resonance contribution. Note that, L_3 is renormalization-scale invariant.

Let us start discussing results obtained from five different fits to the phase-shift data. Best fit parameters and pole properties are compiled in Table I, while predicted phase shifts and SRS amplitudes are depicted in Figs. 5, 6, and 7. In the first fit (**A**), we take the SU(3) Gasser-Leutwyler parameters $L_i^r(\mu = m_\rho)$ from the $\mathcal{O}(p^4)$ $K_{\ell 4}$ fit compiled in Table 2 of Ref. [67].[18] A best fit to data using, instead, the central values of the main $\mathcal{O}(p^6)$ fit of Ref. [67] leads to a χ^2/dof more than twice larger than that of fit **A**. This is not entirely surprising, since we are only considering here one-loop chiral logarithms, besides those required to restore exact unitarity, in the $\pi\pi$ amplitudes. In the four other fits (**B.1**, **B.2**, **B.1-2** and **B.3**), we assume that complete resonance saturation occurs, the corresponding scale (or scales) where it holds is fitted to data. In the fit **B.1-2**, we fix μ_V^{RS} to the value obtained in fit **B.1** and we fit μ_S^{RS} and m_S to data. Besides in the fit **B.3**, we force $m_S = m_V$ in the SRA amplitude, and fit this common mass to the data. We explore this possibility because it is suggested from our previous discussion on short-distance conditions in Eqs. (31) and (32). The $m_S = m_V$ constraint was deduced in Ref. [22] as well, when the one-loop SU(2) ChPT amplitude, unitarized with the Inverse Amplitude Method (IAM), was required to be consistent with the SRA.

Since in the SRA amplitudes we have explicitly incorporated one vector an one scalar poles, we expect at least one pole in each of the $I = J = 0$ and $I = J = 1$ sectors. Because of the re-summation in Eq. (59), the pole positions will change with respect to those of the bare ones ($s = m_V^2$ and $s = m_S^2$) and the resonances will acquire a width that accounts for their two-pion decay. In addition, as we will see, some other poles are generated as well in the SRS of the scattering amplitudes. The five fits have reasonable values of χ^2/dof, though in the $I = J = 1$ channel **B**-type fits lead to a better agreement with data than fit **A**. The major improvement occurs at the higher end of the fitted region, and it is due to the the tail of a second resonance located at around 1.4 GeV (see Fig. 7) that it is generated in the **B** schemes. The relation $g_\rho^2 = m_\rho^4/(6f^2)$, deduced from the KSFR prediction $\Gamma_\rho = m_\rho^3/(96\pi f_\pi^2)$, is satisfied within 3% accuracy. This is because the chiral logarithms are almost negligible in the ρ-meson channel, and indeed at order $\mathcal{O}(p^4)$ they cancel out for the SU(2) massless pion theory [22].

Besides, it is also interesting to compare the leading–N_C values of the residues, as displayed by Eq. (28), with the corresponding ones *after* unitarization, given in Table I. Using the input values one gets $|g_V| \sim 2600$ MeV, in excellent agreement with the

[18] In units of 10^{-3}, $L^r_{1,2,3,4,5,6,8}(\mu = m_\rho) = 0.46,\ 1.49,\ -3.18,\ 0.,\ 1.46,\ 0.$ and 1.08, respectively. For simplicity in the analysis, we have ignored the errors on these parameters, since they do not affect the main conclusions of this work.

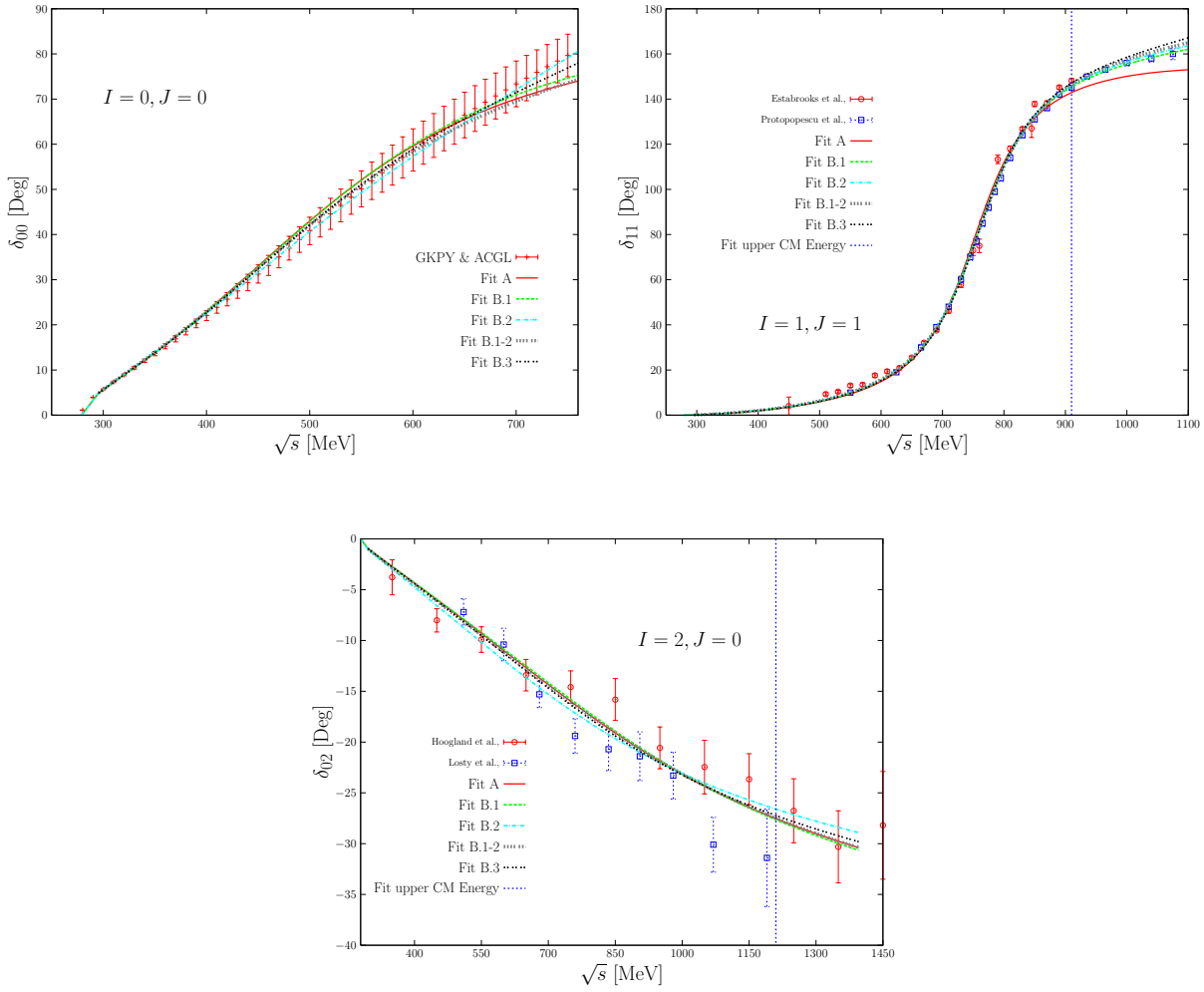


FIG. 5: Theoretical predictions for the phase shifts obtained from fits **A**, **B.1**, **B.2**, **B.1-2** and **B.3**. Fitted data from Refs. [63, 64] ($I = 1, J = 1$) and [65, 66] ($I = 2, J = 0$) are also displayed. In the isoscalar-scalar ($I = 0, J = 0$) channel, the used average of the results of Refs. [61, 62] is shown, as well.

values for $|g_\rho|$ quoted in the table that range in the interval $2400 - 2500$ MeV. For the scalar resonance the rather stable values for $|g_\sigma| \sim 3000 - 3100$ MeV can only be reproduced by Eq. (28) if $m_S = m_V$ (Fit **B.3**). Indeed, for the **B.3** fitted $m_S = m_V$ mass, we find $|g_S| \sim 3000$ MeV. For completeness, let us mention that the residue of the σ resonance has also been deduced from the $\sigma \to \gamma\gamma$ decay [68], yielding $g_\sigma = 3204(28) + \mathrm{i}\,1588(14)$ MeV, i.e. $|g_\sigma| = 3580(30)$ MeV. The result from Roy equations yields $|g_\sigma| = 3300(300)$ MeV [69]. Using the UFD and CFD parameterizations from [34] yields $g_S = 3735(61) + \mathrm{i}\,874(3)$ MeV and $g_\sigma = 3742(60) + \mathrm{i}\,874(6)$ MeV or, equivalently, $|g_\sigma| = 3836(85)$ MeV and $|g_\sigma| = 3843(84)$ MeV respectively, while in the most recent analysis based in GKPY equations, a value of $|g_\sigma| = 3590(120)$ MeV is quoted [4].

Moreover, the scalar-isoscalar phase shifts are significantly better described when the complete resonance saturation of the L_i^r occurs at two different scales fitted to data (fit **B.2**). In this latter case, mass and width of the $f_0(600)$ or σ resonance compare also well with the results of Caprini et al. [2].[19] The properties of the σ resonance are strongly influenced by chiral logarithms [22]. In this scalar-isoscalar channel, we will keep track of a second resonance, which cannot be identified with the $f_0(600)$ and that we will label as *scl*. There exist two types of scenarios: i) for fits **A**, **B.1** and **B.3**, this second pole appears well above m_S (1 GeV for the first two fits and 0.738 GeV for the last one) and it is relatively narrow, and ii) for fits **B.2** and **B.1-2**, it is placed below m_S (1 GeV and 1.295 GeV, respectively) and it is quite wide ($\Gamma \geq 600$ MeV). In the case of the fit **B.2**, the effects of

[19] Bear in mind that in the $I = J = 0$ sector we do not fit directly the Roy equation results of Ref. [61], used in the work of Caprini et al., but rather we take an average of these results with those obtained by Yndurain and collaborators in Ref. [62]. The recent re-analysis [34] provides errors fully compatible with this assumption.

	A	**B.1**	**B.2**	**B.1-2**	**B.3**
C_{00}	-0.0210 (5)	-0.0218 (9)	-0.0278 (18)	-0.0283 (18)	-0.0144 (5)
C_{11}	-0.02054 (11)	-0.01996 (11)	-0.01979 (12)	-0.01968 (12)	-0.0108 (9)
C_{02}	-0.0594 (19)	-0.0588 (20)	-0.0621 (17)	-0.0593 (19)	-0.0606 (18)
μ_V^{RS} (MeV)	770 (fixed)	693 (26)	474 (16)	693 (fixed **B.1**)	520 (21)
μ_S^{RS} (MeV)	770 (fixed)	μ_V^{RS}	1550 (180)	1190 (130)	μ_V^{RS}
m_S (MeV)	1000 (fixed)	1000 (fixed)	1000 (fixed)	1295 (40)	738 (3)
m_V (MeV)	770 (fixed)	770 (fixed)	770 (fixed)	770 (fixed)	m_S
χ^2/dof	3.5	2.4	2.0	2.0	2.2
contrb. χ^2	25/323/21	26/203/22	5/178/20	17/171/20	12/193/20
$r_{12}, r_{13}, r_{14}, r_{15}$	0, 0,-,-	0.06, 0.13, 0.80, -	0.04, 0.05, 0.43, 0.20	0.09, -0.01, 0.47, -0.05	0.20, 0.08, 0.51, -0.20
r_{23}, r_{24}, r_{25}	0,-,-	0.01, 0.07, -	-0.02, -0.12, 0.21	-0.01, 0.29, 0.27	-0.02, -0.20, -0.99
r_{34}, r_{35}	-,-	0.16, -	0.14, -0.10	-0.03, -0.03	0.15, 0.02
r_{45}	-	-	-0.59	0.60	0.22
m_ρ (MeV)	749.1 (4)	752.6 (5)	754.0 (5)	754.8 (6)	754.6 (7)
Γ_ρ (MeV)	144.5 (3)	150.4 (4)	152.0 (4)	153.1 (5)	149.5 (4)
$\lvert g\rvert_\rho$ (MeV)	2404 (4)	2490 (5)	2515 (5)	2534 (7)	2504 (6)
$\sqrt{s_\sigma}$ (MeV)	$(451 \pm 2, -i234 \pm 1)$	$(453 \pm 4, -i238 \pm 4)$	$(423 \pm 6, -i267 \pm 3)$	$(442 \pm 4, -i248 \pm 2)$	$(446 \pm 4, -i246 \pm 4)$
$\lvert g\rvert_\sigma$ (MeV)	3005 (21)	3080 (70)	3070 (120)	3100 (50)	3070 (90)
m_{scl} (MeV)	1340 (40)	1600^{+0}_{-1200}	772 (6)	1020^{+70}_{-650}	1030 (50)
Γ_{scl} (MeV)	117^{+22}_{-0}	300^{+300}_{-0}	580^{+120}_{-0}	1070^{+240}_{-0}	200^{+70}_{-0}
$\lvert g\rvert_{scl}$ (MeV)	2800 (300)	4700^{+0}_{-1700}	2980 (100)	2940 (120)	3300^{+500}_{-400}

TABLE I: Best fit parameters and pole properties (statistical uncertainties on these latter quantities define 68% confidence-level regions, induced by the corresponding Gaussian correlated errors of the different fit parameters). The three C_{IJ} parameters are always fitted to data, and in addition $\mu_V = \mu_S$, μ_V and μ_S, μ_S and m_S, and $\mu_V = \mu_S$ and $m_V = m_S$ are also adjusted in the case of fits **B.1**, **B.2**, **B.1-2** and **B.3**, respectively. In the row labeled as *contrb.*, the contributions to the χ^2 of the different $(I = J = 0)/(I = J = 1)/(I = 2, J = 0)$ sectors are displayed. Besides, r_{ij} are Gaussian correlation coefficients between parameters i and j. Note that the dispersive data analyses based in Roy [2] and GKPY [4] equations predict for $\sqrt{s_\sigma} = (441^{+16}_{-8}, -i272^{+9}_{-12})$ MeV and $(457^{+14}_{-13}, -i279^{+11}_{-7})$ MeV respectively, while the Review of Particle Properties [51] quotes $m_\rho = 775.49 \pm 0.34$ MeV and $\Gamma_\rho = 149.1 \pm 0.8$ MeV.

this resonance (*scl*) on the phase shifts, in the higher end (600-750 MeV) of the fitting range, are appreciable and considerably improve the achieved description (see Figs. 5 and 6). A different question is whether or not such a wide state, below 1 GeV, does have a correspondence with any physical state or it is just an artifact of the fitting procedure. We should note that a state with these features has not been reported neither in the Roy equation analysis of Ref. [69], nor in the most recent work based in the GKPY equations of Ref. [4]. As we shall see in the next subsection, the $N_C \gg 1$ behaviour of the $\sigma-$pole obtained from the **B.2** fit is radically different to that inferred from the **A, B.1** and **B.3** schemes. That is the reason why we have proposed the fit **B.1-2**, with the intention of testing to what extent the dependence on N_C of the $\sigma-$resonance properties is determined by the existence of this possible artifact[20]. In the fit **B.1-2**, where the scale μ_V^{RS} is fixed to the result of fit **B.1** and the value of m_S is adjusted to the data, the second scalar resonance shows up above 1 GeV, and as we will discuss below, it leads to qualitatively the same N_C dependence of the $f_0(600)$ mass and width as the fit **B.2** does.

VI. RESULTS FOR $N_C > 3$

We extrapolate the amplitudes to $N_C > 3$, by means of the N_C dependence

$$A^{\rm SRA+ChPT}(s,t,u)\Big|_{N_C\geq 3} = \frac{3}{N_C} A^{\rm SRA}(s,t,u)\Big|_{N_C=3} + \left(\frac{3}{N_C}\right)^2 \left(A^{\rm ChPT}(s,t,u) - A_4^{\rm SRA}(s,t,u)\right)\Big|_{N_C=3}, \qquad (67)$$

[20] The minimization procedure, involving also the election of the parameters which are fitted to data, is not completely unique, and there exist obviously different local minima. Some of them might not have a proper physical interpretation. Bearing this in mind, we can not discard the existence of artifacts.

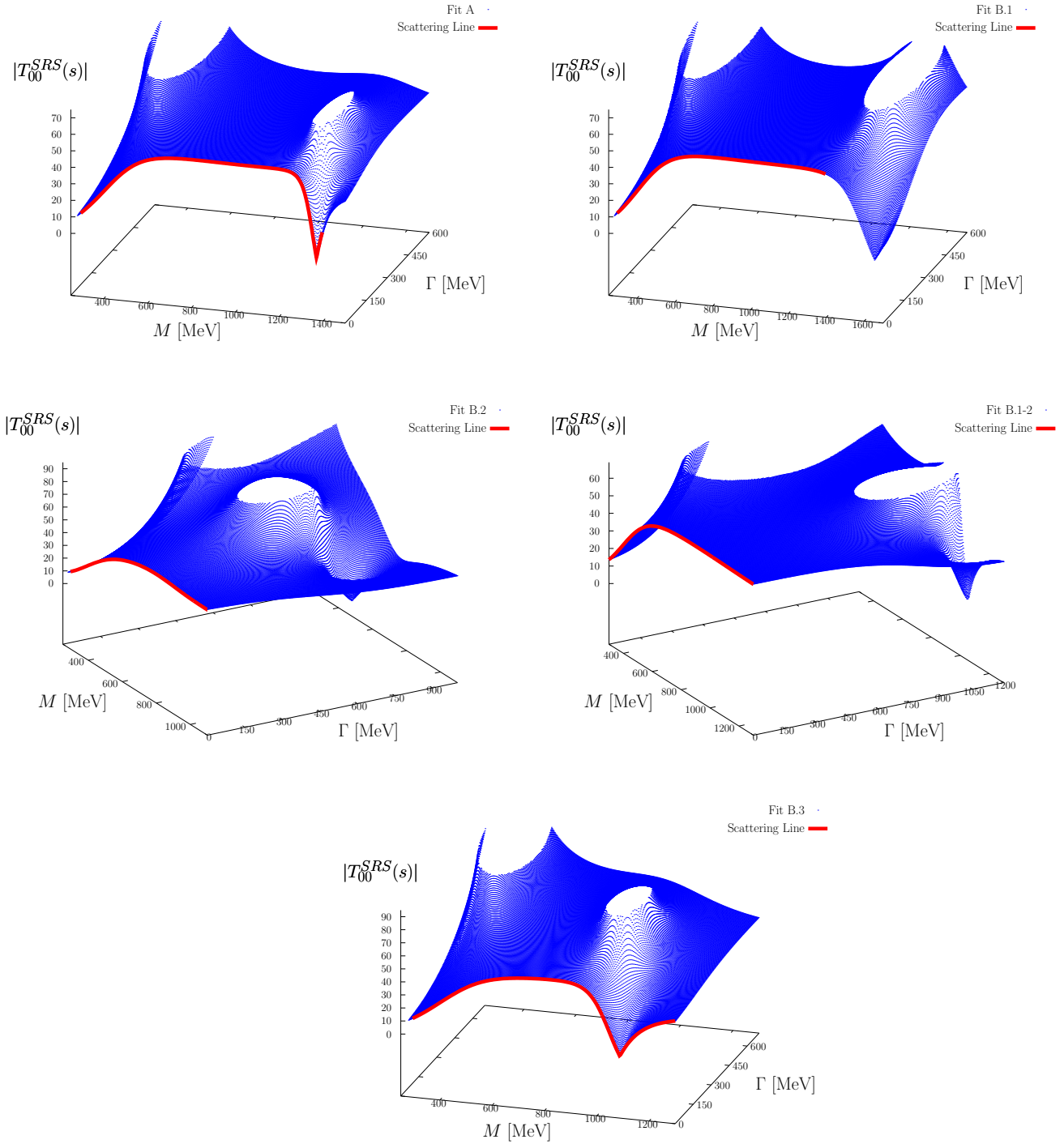


FIG. 6: Modulus of the SRS $T_{00}(s)$ amplitude, as a function of complex s ($s = M^2 - iM\Gamma$) taken in the fourth quadrant, for fits **A**, **B.1**, **B.2**,**B.1-2** and **B.3**. In all plots the physical scattering line ($\Gamma = 0$) is also depicted.

and the scaling law of Eq. (62). $N_C > 3$ results are depicted in Figs. 8, 9 and 10.

In what the ρ meson properties concerns, we observe that for all five fits examined here (Fig. 8), both mass and width behave as expected from a $q\bar{q}$ picture. Thus m_ρ, that did not deviate at $N_C = 3$ much from m_V, quickly approaches to m_V, while Γ_ρ decreases like $1/N_C$, as the number of colors increases. This is not by any means a new result, and in the past other authors have already reached, within an unitarized ChPT scheme, this conclusion [6, 21]. Indeed, in a previous work [22], the same result was obtained starting from the one-loop SU(2) ChPT amplitude for massless pions and using, as in Refs. [6, 21], the IAM to

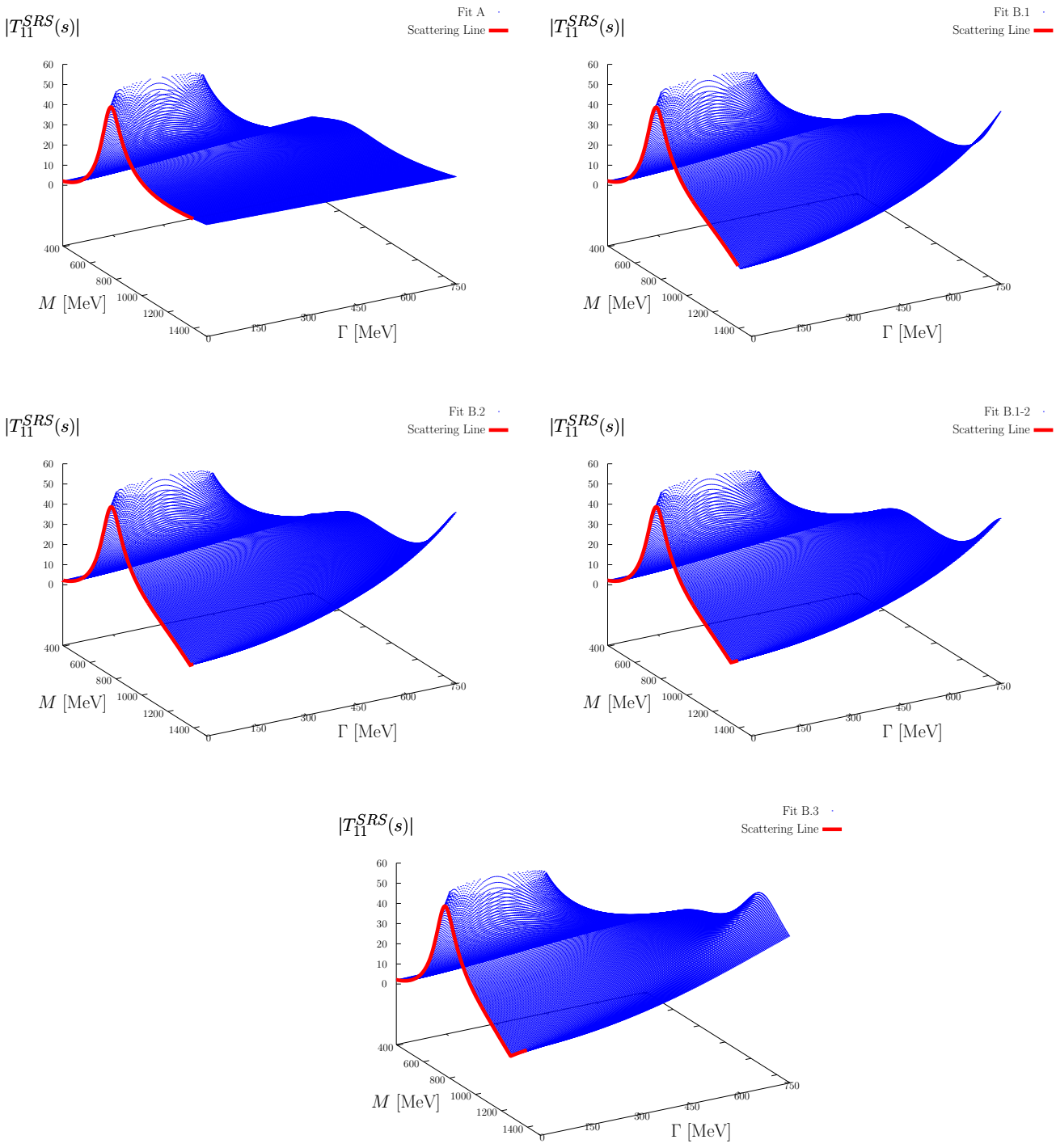


FIG. 7: Modulus of the SRS $T_{11}(s)$ amplitude, as a function of complex s ($s = M^2 - iM\Gamma$) taken in the fourth quadrant, for fits **A**, **B.1**, **B.2**, **B.1-2** and **B.3**. In all plots the physical scattering line ($\Gamma = 0$) is also depicted.

restore elastic unitarity. However, results here are more robust, because in previous works the leading $1/N_C$ terms appearing beyond $\mathcal{O}(p^4)$ [6, 22] or $\mathcal{O}(p^6)$ [21] were simply ignored. Note that the constraint $m_V = m_S + \mathcal{O}(1/N_C)$, deduced in Ref. [22] when the one-loop unitarized $\pi\pi$ amplitude was required to be consistent with the SRA, does no longer necessarily hold here, and we could still have both parameters to be independent (fits **A**, **B.1**, **B.2** and **B.1-2**). Though this could be because we keep here all $1/N_C$ terms at all chiral orders, it might also happen that the above constraint was just an artifact of the IAM used in [22] to unitarize the amplitudes. Nevertheless, we should note that fit **B.3**, where the constraint $m_V = m_S$ is enforced leads to

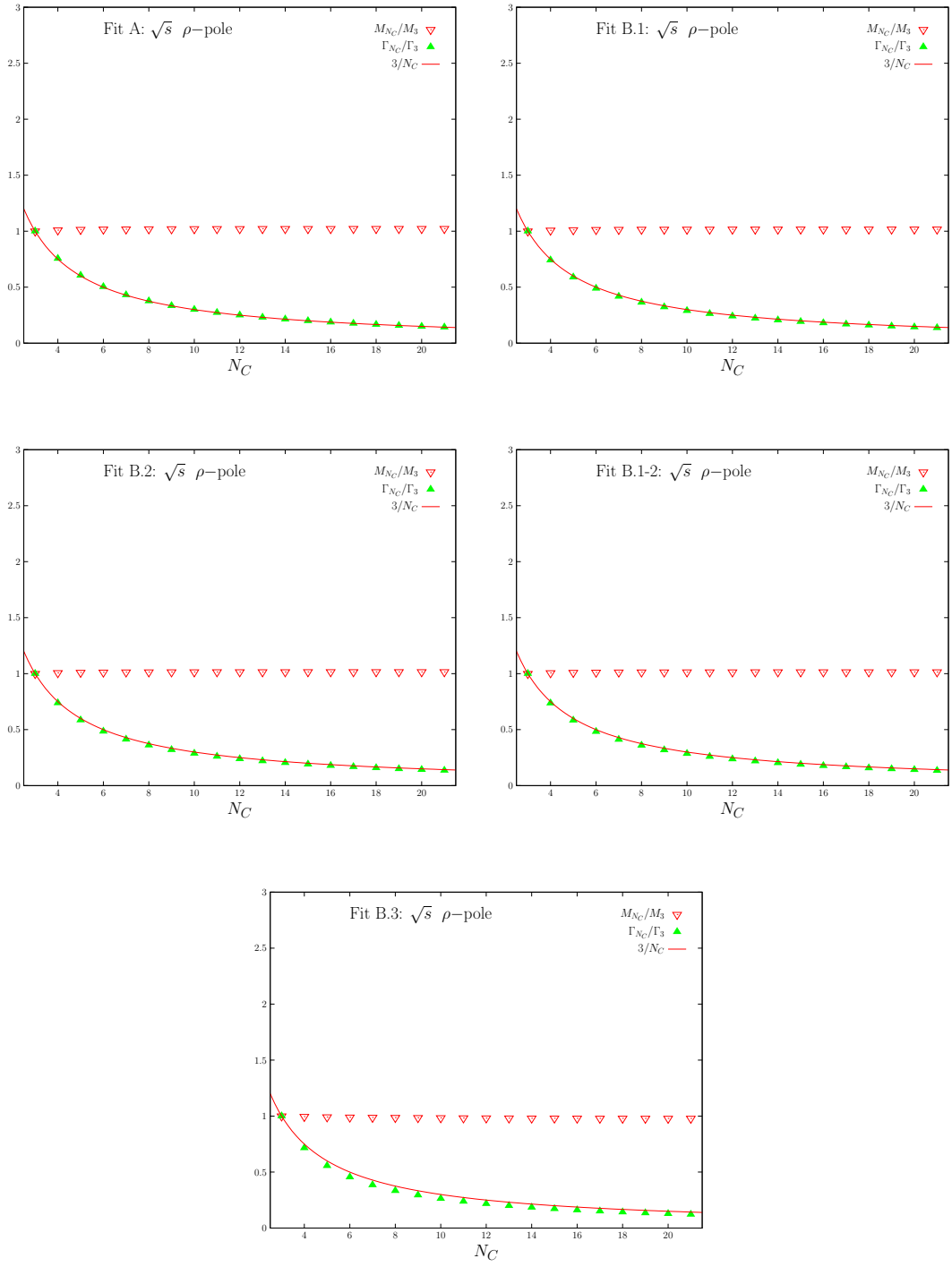


FIG. 8: N_C dependence of the ρ pole position for the various fits described in the text. Empty [filled] triangles stand for $\mathrm{Re}\sqrt{s_\rho}$ [$-2\mathrm{Im}\sqrt{s_\rho}$] in units of the $N_C = 3$ values (M_3 and Γ_3), with s_ρ the SRS pole position (located in the fourth quadrant) for the different N_C values.

phenomenologically acceptable results as well.

Let us move on, and discuss now the scalar-isoscalar channel. For sufficiently large N_C, and since unitarization corrections are subleading, we should end up with just the unique resonance (of mass m_S) included in the SRA irreducible amplitude, while the effects of the second resonance must disappear. We see in Figs. 9 and 10 that this is effectively the case. However, now it is difficult to draw robust conclusions and the resonance that survives depends on the fit procedure.

In the case of the fits **A**, **B.1** and **B.3**, we see that the resonance identified as the $f_0(600)$ for $N_C = 3$ becomes the SRA pole,

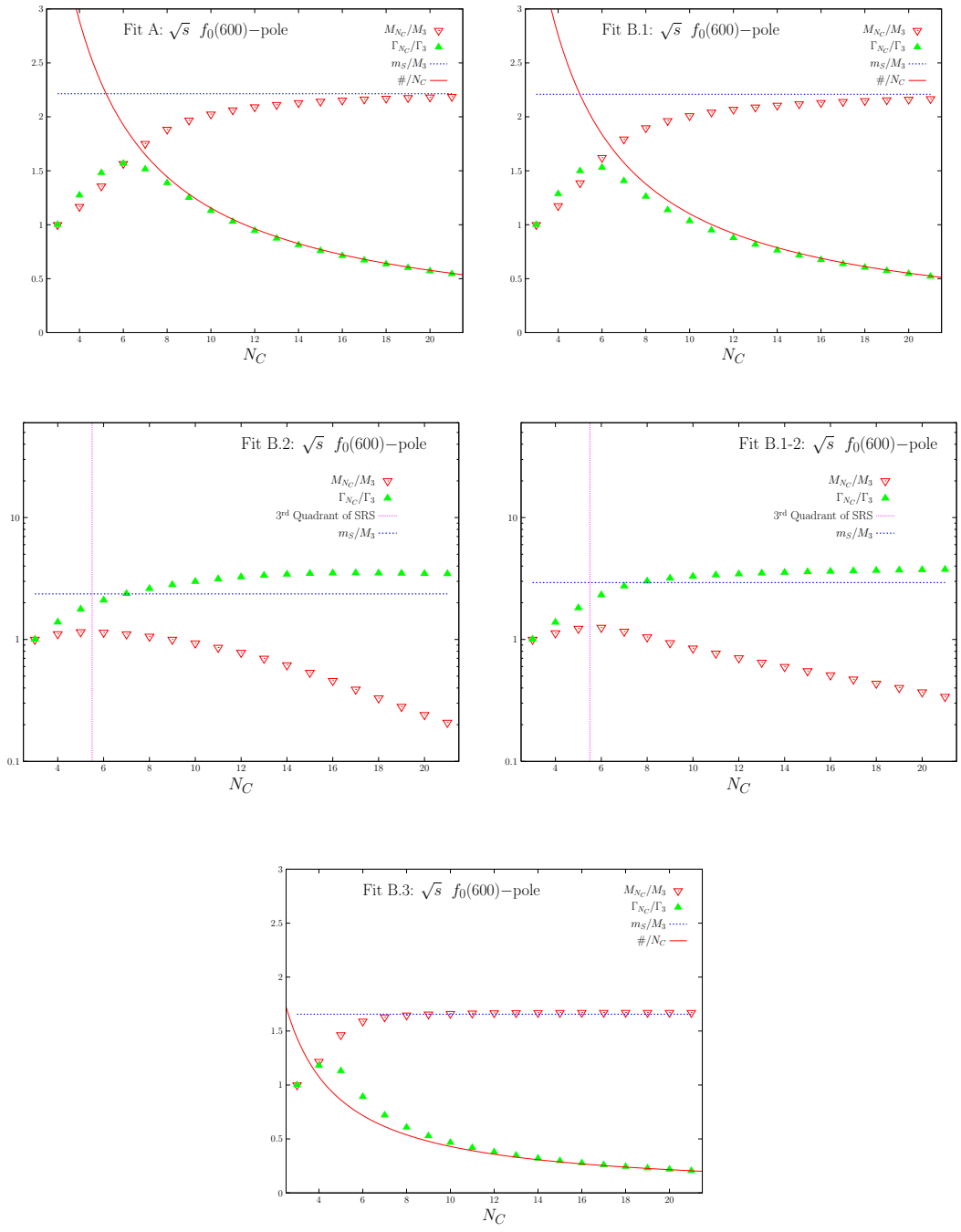


FIG. 9: Same as Fig. 8, but for the σ pole. In addition, the horizontal line indicates the mass of the scalar resonance included in the SRA amplitude (1 GeV for fits **A**, **B.1** and **B.2**, 0.738 GeV for the fit **B.3** and 1.295 GeV in the case of the fit **B.1-2**). For values of N_C located at the right of the vertical line in the **B.2** and **B.1-2** panels, the pole s_σ appears in the third quadrant, instead of in the fourth one, and thus, the singularity does not have a clear physical interpretation.

with mass m_S when N_C is sufficiently large. There is a first transition region for values of N_C close to 3, where both the mass and width increase with N_C, but above $N_C = 6-8$ the resonance width starts decreasing like $1/N_C$, and the mass approaches to the limiting m_S value. The behavior showed in the two upper panels of Fig. 9 is almost identical to that of the right upper panel of Fig. 1 in the two-loop analysis of [21]. The authors of this latter reference conclude that in the case of the σ resonance, there exists a mixing with a $q\overline{q}$ sub-dominant component, arising as loop diagrams become more suppressed at large N_C. The nature of the σ resonance in the real world ($N_C = 3$) would be totally different to that of the ρ meson, being it mostly governed by chiral logarithms stemming from unitarity and crossing symmetry [22], justifying the widely accepted nature of the σ as a

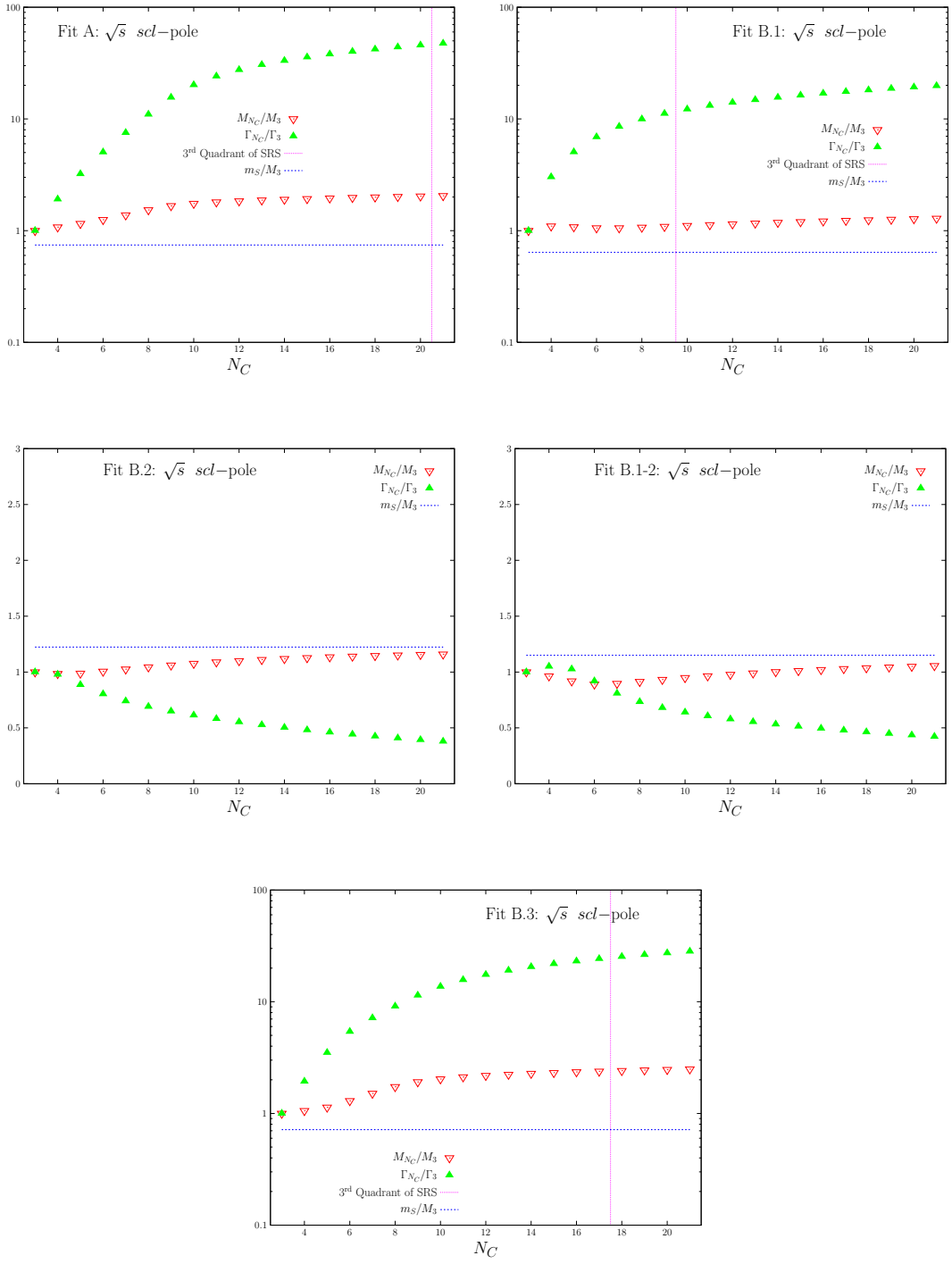


FIG. 10: Same as Fig. 8, but for the *scl* pole. Now, poles appear in the third quadrant for fits **A**, **B.1** and **B.3**.

dynamically-generated meson. However, within this scenario, for sufficiently large $N_C > 10$, the structure of both (σ and ρ) resonances is similar. As pointed out recently in Ref. [30], this solves the seeming paradox of how a distinctive nature for the ρ and σ at $N_C = 3$ is reconciled with semi-local duality at larger values of N_C. Semi-local duality requires the contribution of these

two resonances to the $\pi^+\pi^-$ elastic cross section to cancel[21] "on average", since this process is purely isospin 2 in the t-channel, and there are no isotensor resonances at low energies.

In what respects to the second resonance found in the scalar-isoscalar channel, we see in Fig. 10 that for fits **A**, **B.1** and **B.3**, it follows a totally different pattern with increasing N_C. Indeed, it becomes wider and wider and from one value of N_C on, the pole s_{scl} turns out to be located in the third quadrant, though $\sqrt{s_{scl}}$ still lies in the fourth quadrant, with Re $s < 0$ (where the path integral for the resonance field would not be well defined) and its effects on the scattering disappear. We would like to mention that in Ref. [29] poles in the SRS are being searched in the variable $\sqrt{s}$. That could be inappropriate as we pointed out in Ref. [22], and we reiterate here. This is because, as mentioned above, there are situations where $\sqrt{s_R}$ lies on the fourth quadrant of the SRS, but however s_R has passed to the third quadrant and thus its meaning becomes unclear. This phenomenon, which can only happen for broad resonances, was also illustrated in Fig. 1 of [22], and it is precisely what happens for the σ meson case in Ref. [29] (see the Fig. 10 in that reference). The conclusion of Ref. [29] that the σ meson moves far away in the complex plane for large N_C overlooks the fact that it does so in the third quadrant of the complex plane.

The recent work of Ref. [70] might contradict the findings for the σ resonance deduced from fits **A**, **B.1** and **B.3**, which in turn seem compatible with those obtained in the two-loop analysis of Ref. [21]. In [70], instead, emerges a picture more consistent with that outlined in the one-loop analysis of Ref. [6]. Within the unitarized quark model proposed by Törnqvist [71], the authors of [70] find that the whole low-energy scalar spectrum below 2 GeV, except for a possible glueball $f_0(1710)$, could be described in one consistent picture, with the bare "$q\bar{q}$ seeds" dressed by the hadron loops. In this model, the σ resonance is generated as a pole of the S matrix and has no correspondence with any of the bare $q\bar{q}$ seeds included in the scheme. Indeed, the σ resonance runs away from the real axis on the complex s plane when N_C increases. However, following Ref. [30], this scenario might not be compatible with semi-local duality, when the number of colors is sufficiently high. Besides, we should note that, in sharp contrast with the work here, it is not clear whether the $\pi\pi$ amplitudes used in Ref. [70] contain or not all the leading $1/N_C$ contributions and thus, the analysis of the behavior of the resonance properties when N_C is larger than 3 is not fully meaningful.

The qualitative N_C behavior of the two resonances found in the scalar-isoscalar sector is substantially different when one looks into the results of the fits **B.2** and **B.1-2** (middle panels of Figs. 9 and 10). There, the role played by the $N_C = 3$ σ and *scl* resonances is interchanged. Thus, the $q\bar{q}$ component of the σ seems to be absent, and the $f_0(600)$ pole becomes wider and moves into the third quadrant above $N_C > 5$. Indeed, now the behavior showed by this pole is quite similar to that displayed for the σ in the right panel of Fig.4 of Ref. [70]. On the other hand, as can be appreciated in the middle panels of Fig. 10, the second $I = J = 0$ resonance now becomes the scalar SRA pole included in our amplitudes. Presumably, at high N_C it would become more delta-function-like, as the ρ pole would, and it would likely provide the needed cancellations with the contribution of this latter resonance in the elastic $\pi^+\pi^-$ amplitude [30].

A recent study [72] describes an accidental symmetry of the full Regge tower of radially excited 0^{++} states, $M^2 = an + m_\sigma^2$. Remarkably, the states generating doublets with excited pion states are $f_0(600) \leftrightarrow \pi_0(140)$, $f_0(1370) \leftrightarrow \pi_0(1300)$, $f_0(1710) \leftrightarrow \pi_0(1800)$, $f_0(2100) \leftrightarrow \pi_0(2070)$ and $f_0(2330) \leftrightarrow \pi_0(2360)$, whereas the other scalar states $f_0(980)$, $f_0(1500)$, $f_0(2020)$ and $f_0(2200)$ are not degenerate with other mesons with light u and d quarks. Arguments have been put forward as to identify the $f_0(980)$ as a would-be glueball in the large–N_C limit. As it is well known, glueballs are more weakly coupled to mesons, $\mathcal{O}(1/N_C)$, than other mesons, $\mathcal{O}(1/\sqrt{N_C})$. This is supported by the rather small width ratio which yields $\Gamma_f/\Gamma_\sigma \sim (g^2_{f\pi\pi} m_f^3)/(g^2_{\sigma\pi\pi} m_\sigma^3) \sim 1/N_C$, and for $m_\sigma \sim 0.8$ MeV a ratio $g_{\sigma\pi\pi}/g_{f\pi\pi} \sim \sqrt{N_C}$ is obtained.

Our analysis can be improved along several lines. Firstly, one might extend the chiral analysis to include two-loop results. Secondly, our conclusions might be modified when coupled channels incorporating $\bar{K}K$ effects are taken into account. We have given arguments why we do not expect that this might be important as long as we remain in the sub-threshold region, where all KK effects should be included as $1/N_C$ corrections to the counter-terms.

VII. CONCLUDING REMARKS

We summarize the conclusions of this work. First, we have constructed $\pi\pi$ amplitudes that fulfill exact elastic unitarity, account for one-loop ChPT contributions and include all leading terms, within the SRA, in the $1/N_C$ expansion. These amplitudes have been successfully fitted to $I = J = 0$, $I = 2, J = 0$ and $I = J = 1$ phase shifts. Next, we have looked for poles in the SRS of the amplitudes, and discussed their properties. Since all leading $1/N_C$ terms are taken into account, this scheme is much more appropriated to discuss the N_C dependence of the σ and ρ masses and widths than previous ones, where the leading $1/N_C$ terms appearing beyond $\mathcal{O}(p^4)$ [6, 22] or $\mathcal{O}(p^6)$ [21] were neglected. The recent work of Ref. [29] does not identify correctly the leading $1/N_C$ term, and hence the conclusions of this reference in the large–N_C limit need some revision.

[21] Note however, that such a statement requires an extrapolation of the Regge behavior to somehow low energies. For that end, the authors of Ref. [30] use Regge trajectories for the variable $(\nu - 2m_\pi^2 - t/2)$ to ensure that the imaginary part of the extrapolated Regge amplitude vanishes at threshold.

Robust conclusions are drawn in the case to the ρ resonance, and we confirm here that it is a stable meson in the large–N_C limit, as pointed out by other authors in the past. In the scalar-isoscalar sector, the overall scenario looks like somehow less predictive, since we cannot firmly conclude whether or not the $N_C = 3$ $f_0(600)$ resonance completely disappears at large N_C or it has a sub-dominant component in its structure, which would become dominant when the number of colors gets sufficiently high. Unfortunately, this depends on the chosen procedure (**A**, **B.1** and **B.3** or **B.2** and **B.1-2**) to fit the phase-shift data. However, it becomes clear the predominant di-pion component of this pole for $N_C = 3$, and that the SRA delta-function-like pole, that always appears in the $N_C \gg 1$ limit, might help to keep the whole scheme compatible with semi-local duality. Nevertheless, this needs to be quantitatively checked elsewhere.

Acknowledgments

We thank J.R. Peláez, J. Ruiz de Elvira and J.J. Sanz-Cillero for useful communications. This research was supported by DGI and FEDER funds, under contracts FIS2008-01143/FIS, FPA2007-60323 and the Spanish Consolider-Ingenio 2010 Programme CPAN (CSD2007-00042), by Junta de Andalucía contract FQM0225, by Generalitat Valenciana under contracts PROMETEO/2008/069 and PROMETEO/2009/0090, and it is part of the European Community-Research Infrastructure Integrating Activity "Study of Strongly Interacting Matter" (acronym HadronPhysics2, Grant Agreement n. 227431), under the Seventh EU Framework Programme. A.P. acknowledges the support of the Alexander von Humboldt Foundation.

[1] M. H. Johnson and E. Teller, Phys. Rev. **98**, 783 (1955).
[2] I. Caprini, G. Colangelo, and H. Leutwyler, Phys. Rev. Lett. **96**, 132001 (2006), hep-ph/0512364.
[3] R. Kaminski, J. R. Pelaez, and F. J. Yndurain, Phys. Rev. **D77**, 054015 (2008), 0710.1150 [hep-ph].
[4] R. Garcia-Martin, R. Kaminski, J. Pelaez, and J. de Elvira (2011), 1107.1635 [hep-ph].
[5] E. Klempt and A. Zaitsev, Phys. Rept. **454**, 1 (2007), 0708.4016 [hep-ph].
[6] J. R. Pelaez, Phys. Rev. Lett. **92**, 102001 (2004), hep-ph/0309292.
[7] G. 't Hooft, Nucl. Phys. **B72**, 461 (1974).
[8] E. Witten, Nucl. Phys. **B160**, 57 (1979).
[9] G. Ecker, J. Gasser, A. Pich, and E. de Rafael, Nucl. Phys. **B321**, 311 (1989).
[10] G. Ecker, J. Gasser, H. Leutwyler, A. Pich, and E. de Rafael, Phys. Lett. **B223**, 425 (1989).
[11] S. Weinberg, Physica **A96**, 327 (1979).
[12] J. Gasser and H. Leutwyler, Ann. Phys. **158**, 142 (1984).
[13] J. Gasser and H. Leutwyler, Nucl. Phys. **B250**, 465 (1985).
[14] V. Cirigliano et al., Nucl. Phys. **B753**, 139 (2006), hep-ph/0603205.
[15] J. Bijnens, E. Gamiz, E. Lipartia, and J. Prades, JHEP **04**, 055 (2003), hep-ph/0304222.
[16] F. Sannino and J. Schechter, Phys. Rev. **D52**, 96 (1995), hep-ph/9501417.
[17] M. Harada, F. Sannino, and J. Schechter, Phys. Rev. **D54**, 1991 (1996), hep-ph/9511335.
[18] A. Pich (2002), hep-ph/0205030.
[19] J. Nieves and E. Ruiz Arriola, Phys. Lett. **B679**, 449 (2009), 0904.4590 [hep-ph].
[20] Z. X. Sun, L. Y. Xiao, Z. Xiao, and H. Q. Zheng, Mod. Phys. Lett. **A22**, 711 (2007), hep-ph/0503195.
[21] J. R. Pelaez and G. Rios, Phys. Rev. Lett. **97**, 242002 (2006), hep-ph/0610397.
[22] J. Nieves and E. R. Arriola, Phys. Rev. **D80**, 045023 (2009), 0904.4344 [hep-ph].
[23] P. Di Vecchia and G. Veneziano, Nucl.Phys. **B171**, 253 (1980).
[24] E. Witten, Annals Phys. **128**, 363 (1980).
[25] C. Rosenzweig, J. Schechter, and C. Trahern, Phys.Rev. **D21**, 3388 (1980).
[26] R. Kaiser and H. Leutwyler, Eur. Phys. J. **C17**, 623 (2000), hep-ph/0007101.
[27] N. Beisert and B. Borasoy, Phys. Rev. **D67**, 074007 (2003), hep-ph/0302062.
[28] M. Albaladejo, J. A. Oller, and L. Roca, Phys. Rev. **D82**, 094019 (2010), 1011.1434 [hep-ph].
[29] Z.-H. Guo and J. A. Oller (2011), 1104.2849 [hep-ph].
[30] J. Ruiz de Elvira, J. R. Pelaez, M. R. Pennington, and D. J. Wilson (2010), 1009.6204 [hep-ph].
[31] B. Martin, D. Morgan, and G. Shaw, *Pion-pion interactions in particle physics*, vol. 101 (Academic press London, 1976).
[32] F. J. Yndurain (2002), hep-ph/0212282.
[33] J. Nieves and E. Ruiz Arriola, Nucl. Phys. **A679**, 57 (2000), hep-ph/9907469.
[34] R. Garcia-Martin, R. Kaminski, J. Pelaez, J. Ruiz de Elvira, and F. Yndurain, Phys.Rev. **D83**, 074004 (2011), 1102.2183 [hep-ph].
[35] J. R. Pelaez and F. J. Yndurain, Phys. Rev. **D68**, 074005 (2003), hep-ph/0304067.
[36] J. R. Pelaez and F. J. Yndurain, Phys. Rev. **D69**, 114001 (2004), hep-ph/0312187.
[37] S. L. Adler and F. J. Yndurain, Phys. Rev. **D75**, 116002 (2007), 0704.1201 [hep-ph].
[38] D. Black, A. H. Fariborz, F. Sannino, and J. Schechter, Phys. Rev. **D59**, 074026 (1999), hep-ph/9808415.
[39] V. Cirigliano, G. Ecker, H. Neufeld, and A. Pich, JHEP **06**, 012 (2003), hep-ph/0305311.
[40] F. Giacosa, T. Gutsche, V. E. Lyubovitskij, and A. Faessler, Phys. Rev. **D72**, 094006 (2005), hep-ph/0509247.

[41] Z.-H. Guo and J. J. Sanz-Cillero, Phys. Rev. **D79**, 096006 (2009), 0903.0782 [hep-ph].
[42] Z. H. Guo, J. J. Sanz Cillero, and H. Q. Zheng, JHEP **06**, 030 (2007), hep-ph/0701232.
[43] A. Pich, I. Rosell, and J. J. Sanz-Cillero, JHEP **02**, 109 (2011), 1011.5771 [hep-ph].
[44] Z.-H. Guo and P. Roig, Phys. Rev. **D82**, 113016 (2010), 1009.2542 [hep-ph].
[45] G. Ecker, Acta Phys. Polon. **B38**, 2753 (2007), hep-ph/0702263.
[46] F. J. Gilman and H. Harari, Phys. Rev. **165**, 1803 (1968).
[47] S. Weinberg, Phys. Rev. **177**, 2604 (1969).
[48] S. Weinberg, Phys. Rev. Lett. **65**, 1177 (1990).
[49] G. Ecker and C. Zauner, Eur. Phys. J. **C52**, 315 (2007), 0705.0624 [hep-ph].
[50] D. Toublan, Phys. Rev. **D53**, 6602 (1996), hep-ph/9509217.
[51] K. N. et al., J. Phys. **G37**, 075021 (2010).
[52] C. Garcia-Recio, L. Geng, J. Nieves, and L. Salcedo, Phys.Rev. **D83**, 016007 (2011), 1005.0956 [hep-ph].
[53] E. Megias, E. Ruiz Arriola, L. L. Salcedo, and W. Broniowski, Phys. Rev. **D70**, 034031 (2004), hep-ph/0403139.
[54] J. Nieves and E. Ruiz Arriola, Phys. Lett. **B455**, 30 (1999), nucl-th/9807035.
[55] I. Rosell, J. J. Sanz-Cillero, and A. Pich, JHEP **0408**, 042 (2004), hep-ph/0407240.
[56] I. Rosell, J. J. Sanz-Cillero, and A. Pich, JHEP **0701**, 039 (2007), hep-ph/0610290.
[57] A. Pich, I. Rosell, and J. J. Sanz-Cillero, JHEP **0807**, 014 (2008), 0803.1567 [hep-ph].
[58] I. Rosell, P. Ruiz-Femenia, and J. Portoles, JHEP **0512**, 020 (2005), hep-ph/0510041.
[59] J. Portoles, I. Rosell, and P. Ruiz-Femenia, Phys.Rev. **D75**, 114011 (2007), hep-ph/0611375.
[60] J. Nieves and E. Ruiz Arriola, Phys. Rev. **D64**, 116008 (2001), hep-ph/0104307.
[61] B. Ananthanarayan, G. Colangelo, J. Gasser, and H. Leutwyler, Phys. Rept. **353**, 207 (2001), hep-ph/0005297.
[62] F. J. Yndurain, R. Garcia-Martin, and J. R. Pelaez, Phys. Rev. **D76**, 074034 (2007), hep-ph/0701025.
[63] P. Estabrooks and A. D. Martin, Nucl. Phys. **B79**, 301 (1974).
[64] S. D. Protopopescu et al., Phys. Rev. **D7**, 1279 (1973).
[65] W. Hoogland et al., Nucl. Phys. **B126**, 109 (1977).
[66] M. Losty, V. Chaloupka, A. Ferrando, L. Montanet, E. Paul, D. Yaffe, J. Zieminski, et al., Nuclear Physics B **69**, 185 (1974), ISSN 0550-3213.
[67] G. Amoros, J. Bijnens, and P. Talavera, Nucl. Phys. **B585**, 293 (2000), hep-ph/0003258.
[68] J. Bernabeu and J. Prades, Phys. Rev. Lett. **100**, 241804 (2008), 0802.1830 [hep-ph].
[69] H. Leutwyler, AIP Conf. Proc. **1030**, 46 (2008), 0804.3182 [hep-ph].
[70] Z.-Y. Zhou and Z. Xiao, Phys. Rev. **D83**, 014010 (2011), 1007.2072 [hep-ph].
[71] N. A. Tornqvist, Z. Phys. **C68**, 647 (1995), hep-ph/9504372.
[72] E. Ruiz Arriola and W. Broniowski, Phys. Rev. **D81**, 054009 (2010), 1001.1636 [hep-ph].